RESEARCH PAPER

ACTA PHYSIOLOGICA

Routing of Kv7.1 to endoplasmic reticulum plasma membrane junctions

Clara Serrano-Novillo[1] | Irene Estadella[1] | María Navarro-Pérez[1] |
Anna Oliveras[1,2] | Angela de Benito-Bueno[3] | Paula G. Socuéllamos[3] |
Manel Bosch[1,4] | María José Coronado[5] | Daniel Sastre[1,6] | Carmen Valenzuela[3] |
Christian Soeller[7] | Antonio Felipe[1]

[1]Molecular Physiology Laboratory, Departament de Bioquímica i Biomedicina Molecular, Institut de Biomedicina (IBUB), Universitat de Barcelona, Barcelona, Spain

[2]Berlin Institute of Medical Systems Biology (BIMSB), Max Delbrück Center for Molecular Medicine, Berlin, Germany

[3]Instituto de Investigaciones Biomédicas Alberto Sols CSIC-UAM, Madrid, Spain

[4]Scientific and Technological Centers (CCiTUB), Universitat de Barcelona, Barcelona, Spain

[5]Unidad de Microscopía Confocal, Instituto de Investigación Sanitaria Puerta de Hierro-Segovia de Arana (IDIPHISA), Hospital Universitario Puerta de Hierro, Madrid, Spain

[6]Department of Anesthesiology, Pharmacology and Therapeutics, Faculty of Medicine, University of British Columbia, Vancouver, British Columbia, Canada

[7]Department of Physiology, University of Bern, Bern, Switzerland

Correspondence
Antonio Felipe, Molecular Physiology Laboratory, Departament de Bioquímica i Biomedicina Molecular, Institut de Biomedicina (IBUB), Universitat de Barcelona, Barcelona, Spain.
Email: afelipe@ub.edu

Abstract

Aim: The voltage-gated Kv7.1 channel, in association with the regulatory subunit KCNE1, contributes to the I_{Ks} current in the heart. However, both proteins travel to the plasma membrane using different routes. While KCNE1 follows a classical Golgi-mediated anterograde pathway, Kv7.1 is located in endoplasmic reticulum-plasma membrane junctions (ER-PMjs), where it associates with KCNE1 before being delivered to the plasma membrane.

Methods: To characterize the channel routing to these spots we used a wide repertoire of methodologies, such as protein expression analysis (i.e. protein association and biotin labeling), confocal (i.e. immunocytochemistry, FRET, and FRAP), and dSTORM microscopy, transmission electron microscopy, proteomics, and electrophysiology.

Results: We demonstrated that Kv7.1 targeted ER-PMjs regardless of the origin or architecture of these structures. Kv2.1, a neuronal channel that also contributes to a cardiac action potential, and JPHs, involved in cardiac dyads, increased the number of ER-PMjs in nonexcitable cells, driving and increasing the level of Kv7.1 at the cell surface. Both ER-PMj inducers influenced channel function

Clara Serrano-Novillo, Irene Estadella, and María Navarro-Pérez contributed equally to this work.

and dynamics, suggesting that different protein structures are formed. Although exhibiting no physical interaction, Kv7.1 resided in more condensed clusters (ring-shaped) with Kv2.1 than with JPH4. Moreover, we found that VAMPs and AMIGO, which are Kv2.1 ancillary proteins also associated with Kv7.1. Specially, VAP B, showed higher interaction with the channel when ER-PMjs were stimulated by Kv2.1.

Conclusion: Our results indicated that Kv7.1 may bind to different structures of ER-PMjs that are induced by different mechanisms. This variable architecture can differentially affect the fate of cardiac Kv7.1 channels.

KEYWORDS

adaptors, cell surface targeting, ERPMj inducers, potassium channels

1 | INTRODUCTION

Voltage-dependent potassium channels play a role in cardiac action potentials. The Kv7.1 channel coassembles with the KCNE1 β regulatory subunit to mediate the slow delayed rectifier potassium current (I_{Ks}) in the human ventricle.[1,2] The I_{Ks} channel is a major repolarization current in the heart, and mutations in either Kv7.1 or KCNE1 can lead to long QT syndrome.[3] The following are two major topics surrounding the nature of the Kv7.1-KCNE1 association that are subject to intense debate: (i) the stoichiometry of α and β subunits within the complex[4–6] and (ii) the cellular compartment where the association takes place.[7–10] For the first issue, sound evidence indicates that Kv7.1, as a member of the Kv superfamily, forms tetrameric channels that interact with one to four KCNE1 units, resulting in complexes with distinct kinetic properties and different architectures.[4] However, the latter topic still generates intense debate. Accumulating evidence claims that channel proteins associate either at the endoplasmic reticulum or at the plasma membrane. However, recent studies suggest that Kv7.1 and KCNE1 route separately to the cell surface and then interact in endoplasmic reticulum-plasma membrane junctions (ER-PMjs). Advanced technologies demonstrate that while KCNE1 travels to these locations by a canonical anterograde route via the Golgi apparatus, Kv7.1 uses a noncanonical path to reach the plasma membrane.[7,8] Therefore, these ER-PMjs, which are plasma membrane to endoplasmic reticulum contact sites, are hot spots for investigating the I_{Ks} complex interactions.

Cardiac T-tubules are specialized ER-PMjs. In these tubules, the surrounding sarcolemma contacts the sarcoplasmic reticulum (SR) to form characteristic transverse structures that house the ion channel machinery for excitation-contraction (E-C) coupling. T-tubules host ryanodine receptors (RyR) and L-type Ca^{2+} channels (LTCCs) but also K^+ channels that contribute to the

termination of cardiac action potentials.[11] Among these ion channel proteins, Kv7.1 and KCNE1 have been located in these structures.[7,12–14]

In addition to cardiac T-tubules, different types of ER-PMjs exist in different tissues, which involve different scaffold proteins that shape their molecular architecture. Thus, while junctophilins (JPHs) are essential actors in the stabilization and formation of cardiac T-tubules, the voltage-dependent Kv2.1 channel, together with adaptor proteins such as vesicle-associated membrane proteins (VAMPs: VAP A and VAP B) and AMIGO 1, are crucial for proper ER-PMj functioning in neurons.[11,15] Moreover, during the immune system response, the interaction between ORAI channels located in the ER and STIM in the PM promotes the formation of ER-PMjs, which are crucial for the Ca^{2+} signaling cascade during the immune response.[16,17] Therefore, sound studies indicate that in this context, several ER-PMj structures may be generated, which could influence the final fate and function of ion channels. Considering that Kv7.1 routes to ER-PMjs by an unconventional mechanism[7,8] and that Kv2.1, which is important in neurons,[11,15] also contributes to an action potential in the heart,[18] we investigated the molecular mechanisms that define Kv7.1 targeting to these specialized locations. We found that in a series of immortalized cell lines, such as AC16 cardiomyocytes, HEK 293, and COS-7 cells, not only JPHs but also Kv2.1 promote the formation of ER-PMjs. The generation of these structures augmented the migration and localization of Kv7.1 toward these locations. As a result, Kv currents increased. Differential ER-PMj origins altered channel function and dynamics. Without any physical interaction with JPH or Kv2.1, this variation was influenced by the different associations between the channel and scaffold proteins. The Kv7.1 interactome highlighted a number of proteins involved in the lipid raft architecture, which is a hallmark of ER-PMj membranes. Finally, we observed, for the first time, that Kv7.1 associates with VAMPs and AMIGO, which are Kv2.1 partners, and a differential

interaction could influence the final fate of the channel reaching these PM to ER contact sites. Our data are of physiological relevance because they shed light on the mechanism that drives the unconventional migration of Kv7.1 to the PM and ER-PMjs, where it associates with KCNE1 to generate the crucial I_{Ks} current in the heart.

2 | RESULTS

2.1 | Kv7.1 localizes to the plasma membrane and cardiac T-tubules

To characterize the routing mechanism of Kv7.1, we first analyzed the localization of the channel. Kv7.1 was localized in the plasma membrane in HEK 293 cells transfected with Kv7.1-CFP. However, the channel, being an integral plasma membrane protein, exhibited rather limited cell surface colocalization (Figure 1Aa–c). As a result, we speculated that classical cell culture reflected nonnative conditions. Since cardiomyocytes and neurons are polarized cells, we cultured Kv7.1-expressing HEK 293 cells in Transwell permeable supports (TW), allowing cells to have full surface access to the culture medium (Figure 1Ad–f). Under such conditions, Kv7.1 was efficiently distributed throughout the plasma membrane (Figure 1Ag), which was further supported by 3D projections (Figure 1Ba–f) and biotinylation studies (Figure 1Ca,b). These data demonstrated that limited surface staining, usually a characteristic of this channel, is a technical limitation of 2D plastic culture conditions. Our results showed a channel localization of ER-PMjs in HEK 293 cells (Figure 1D) and in cardiac T-tubules stained by RyR, which are specialized sarcolemma-sarcoplasmic reticulum ER-PMjs in cardiomyocytes (Figure 1E).

Several proteins promote the formation and localization of ER-PMjs.[11] While JPHs participate in skeletal and cardiac muscles, the voltage-dependent Kv2.1 channel associates with these ER-PM contact sites in neurons.[11,19] While both proteins were present in the heart, only JPHs (i.e., JPH1) were endogenously expressed in HEK 293 cells (Figure 1F). Therefore, to analyze the effect and mechanism of Kv7.1 binding to ER-PMjs, we engineered human AC16 cardiomiocytes and HEK 293 cells by incorporating either Kv2.1 or JPH4.

2.2 | Kv2.1 and JPH4 promote ER-PMj formation and upregulate plasma membrane Kv7.1 expression

The presence of ER-PMjs in HEK 293 cells was analyzed by transmission electron microscopy (Figure 2). Nontransfected HEK 293 cells contained a limited number of ER-PMjs (Figure 2A,B). The expression of Kv2.1 and JPH4 notably augmented the number and length of these structures (Figure 2C–E). This is a consequence of the specific expression of Kv2.1 and JPH4 because the transfection of Kv7.1 itself did not increase the number of ER-PMjs. JPHs and Kv2.1 facilitate ER-PMj formation in muscles and nerves, and our results demonstrated that this role is further extended to other cell types.

We next evaluated whether an increase in the number of ER-PMjs also upregulated the expression of Kv7.1 at the cell surface (Figure 3). HEK 293 cells were transfected with Kv7.1 in the absence or presence of Kv2.1, JPH4, or both. Indeed, not only Kv2.1 but also JPH4 augmented Kv7.1 targeting to the cell surface (Figure 3A,B). In addition, the presence of both Kv2.1 and JPH4 was somehow additive (Figure 3B). Biotinylation experiments further confirmed that Kv7.1 expression was upregulated at the plasma membrane in the presence of Kv2.1 and JPH4 (Figure 3C,D).

Similar results were obtained by using human AC16 cardiomyocites (Figure 4). AC16 cells expressed endogenous Kv7.1 and JPH4, but not Kv2.1 (Figure 4A,C). In this context, we transfected Kv2.1 and JPH4 and, similar to HEK 293 cells, both inducers increased endogenous Kv7.1 plasma membrane targeting (Figure 4D,E). In addition, Kv7.1 biotinylation studies further supported that both inducers elevated the targeting of Kv7.1 to the plasma membrane (Figure 4F,G). Immunohistochemistry studies in atrial human samples also support the colocalization of Kv7.1 and JPH4, but not Kv2.1 expression (Figure S1).

The Kv7.1 channel routes to the cell surface by an unconventional mechanism – bypassing the Golgi apparatus – which drives the channel via ER-PMjs to the cell membrane.[7,8] Thus, Brefeldin, which suppresses the canonical Golgi-dependent anterograde route, did not alter Kv7.1 ER localization (Figure S2A,B). This finding is specific to the Kv7.1 channel alone since its β-regulatory subunit KCNE1 follows the classical anterograde route via the Golgi, as demonstrated by incubation with Brefeldin (Figure S2C,D). Furthermore, Kv2.1 did not alter the expression of KCNE1 when expressed alone (Figure S2E,F). In this scenario, the transmission electron microscopy results confirmed that Kv7.1 was already present in these structures (Figure 5). Donut-like shapes, representing ER-PMjs, have been visualized when the ER contacts the PM.[19] Our dSTORM images showed that these annular structures always contained Kv7.1. Most structures contained Kv7.1 alone or associated with KCNE1 but never KCNE1 alone, which reinforces that ER-PMjs are hubs for the Kv7.1-KCNE1 association caused by the differential trafficking mechanism of those proteins (Figure S3).

To determine whether Kv2.1- or JPH4-dependent ER-PMjs modulated the activity of Kv7.1, we performed
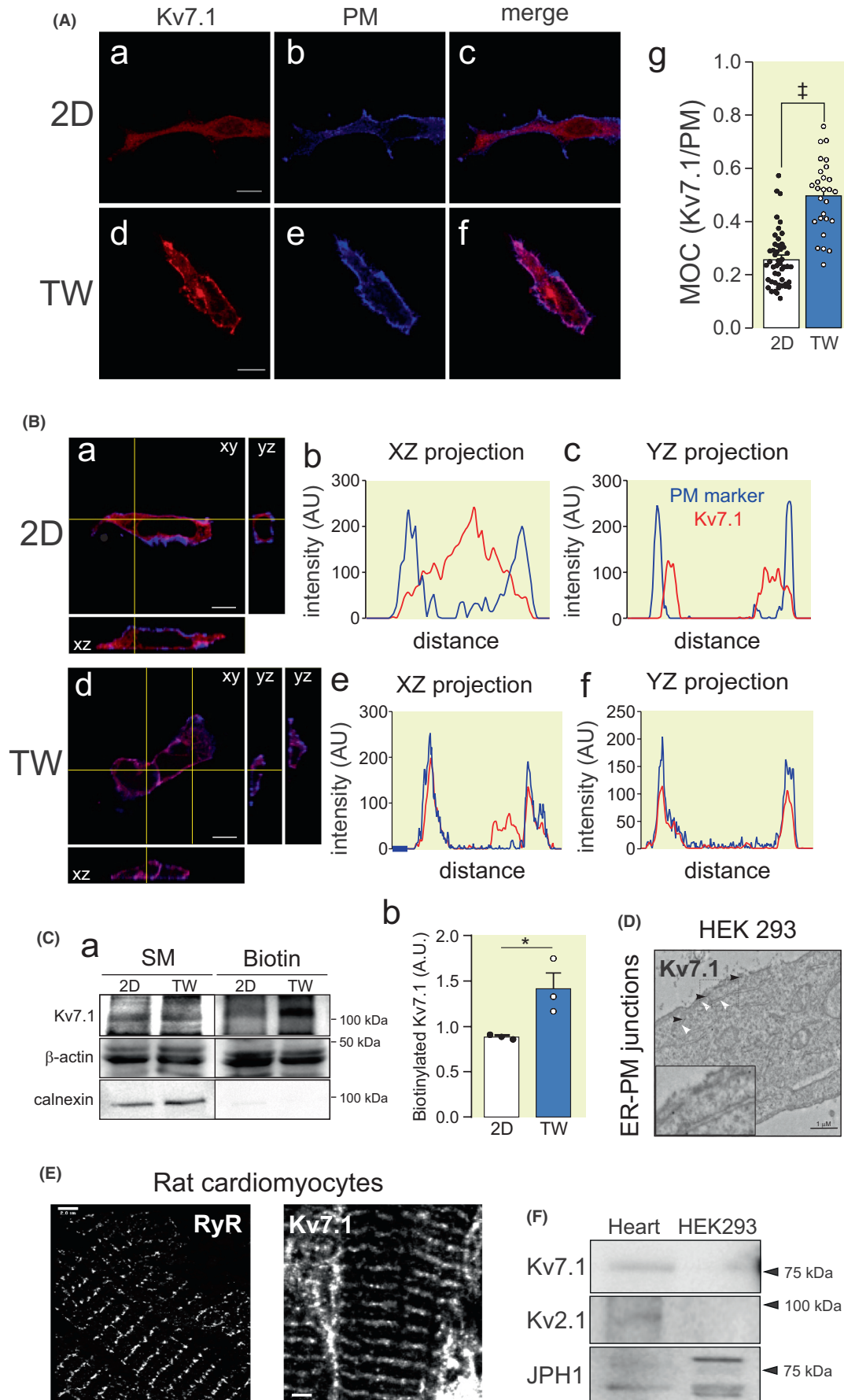
FIGURE 1 Kv7.1 targets the plasma membrane and ER-PMjs in HEK 293 cells and cardiomyocytes. (A–C) HEK 293 cells were transfected with Kv7.1-CFP, and the culture split in 2D non-permeable regular plastic dishes (2D) and Transwell permeable supports (TW) for 48 h. (A) Kv7.1 cell surface expression was upregulated in TW culture devices. Representative images of Kv7.1-CFP (Aa,d in red) and Akt-PH-pDsRed (PM marker) (Ab,e in blue). (Ac,f) Colocalization in magenta. (Aa–c) 2D conventional culture system. (Ad–f) Transwell (TW) culture system. Scale bars: 10 μm. (Ag) Manders' overlapping coefficient (MOC) analysis of Kv7.1 and PM in TW (blue bars) and 2D (white bars) cells. The bar graph represents the mean ± SE. ‡$p < 0.001$ TW vs. 2D cells ($n = 50$ cells, Student's t-test). (B) Kv7.1 whole-cell orthogonal projections. (Ba–c) Optical mid-section (XY) and orthogonal views (XZ, YZ) of representative confocal z-stacks of HEK 293 cells cultured in conventional systems (2D). Side views were reconstructed from the yellow line axis. (Bd–f) Optical mid-section (XY) and orthogonal views (XZ, YZ) of representative confocal z-stacks of HEK 293 cells cultured in the Transwell system (TW). Side views were reconstructed from the yellow line axis. (Bb,c and Be,f) Plot profiles showing the pixel-by-pixel analysis of perpendicular sections (yellow lines) in the XZ and YZ projections in 2D (top panels) and TW (bottom panels) cells. Kv7.1 histogram, in red; PM, in blue. (C) After 48 h of transfection, cells, cultured in 2D and TW, were labeled with biotin to detect plasma membrane Kv7.1 and processed as described in Materials and Methods. Calnexin was used as a negative control. β-Actin was used as a loading control. SM: Starting materials; Biotin: Pull down of biotinylated proteins. (Ca) representative western blot; (Cb) quantification of 3 independent experiments. 2D (white bar) and TW (blue bar). *$p < 0.05$ TW vs. 2D cells (Student's t-test). (D) Representative electron micrograph showing Kv7.1 in ER-PMjs from HEK 293 cells expressing Kv7.1-CFP. CFP was stained by 18 nm gold particles (black arrowheads) located in ER-PMjs, highlighted with white arrowheads (see inset), near the plasma membrane. The scale bar represents 1 μm. (E) Direct stochastic optical reconstruction microscopy (dSTORM) in rat ventricular cardiomyocytes. Left panel, Ryanodine receptor (RyR), a sarcomeric marker that localizes in cardiac T-tubule structures in specific cardiac cell types. Right panel, Kv7.1 staining of the same structures. Scale bars: 2 μm. (F) Expression of Kv7.1, Kv2.1, and JPH1 in rat heart samples and HEK 293 cells. Total crude protein extracts from rat ventricular cardiomyocytes (Heart) and control (nontransfected) HEK 293 cells (HEK 293) were analyzed to determine endogenous protein expression.

patch-clamp studies (Figure 6). Voltage-dependent K⁺ currents elicited in COS-7 cells transfected with Kv7.1 increased in the presence of these two proteins. Similar to HEK 293 cells, Kv2.1 and Kv7.1 increased the expression of Kv7.1 in the cell surface of COS-7 cells (Figure S4). Neuronal Kv2.1 participates in the formation of ER-PMjs, independent of ion channel function. Therefore, we used a nonconducting Kv2.1 mutant (Kv2.1 P404W) to avoid current interference.[20] Although current-less, the capacity of Kv2.1 P404W to increase the number of ER-PMjs was not altered (Figure S5). The presence of ER-PMj inducers (Kv2.1 and JPH4) increased Kv7.1 currents 2- to 3-fold with no changes in steady-state activation (Figure 6A–C). However, the presence of either protein slowed the activation of the channel (Figure 6D), with no changes in de-activation (Figure 6E). Our results indicated that the de novo formation of ER-PMjs upregulated Kv7.1 cell surface expression, which exhibited subtle changes in channel kinetics, suggesting different ER-PMj structures.
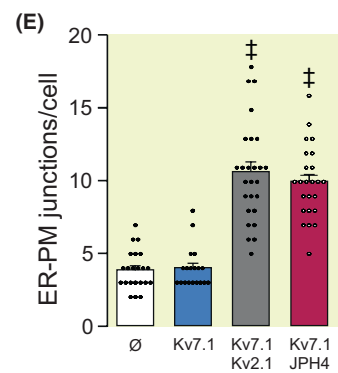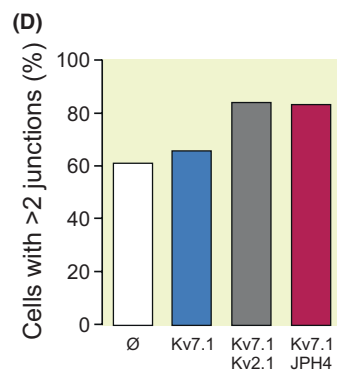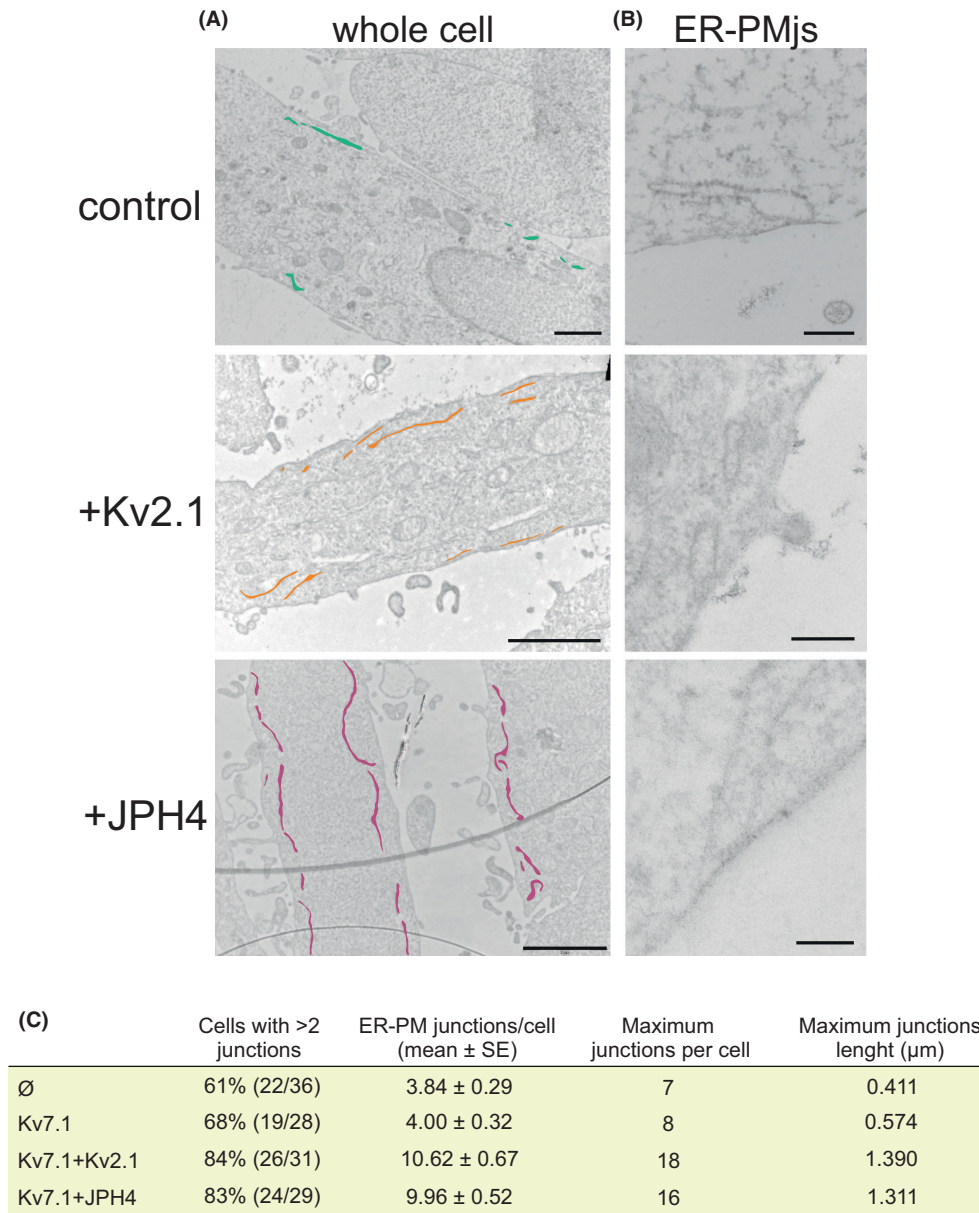
2.3 | The nature of Kv7.1-containing ER-PMjs generated by Kv2.1 and JPH4 is different

Next, we wanted to study mechanisms involved in the binding of Kv7.1 to ER-PMjs. Coimmunoprecipitation experiments and FRET analysis demonstrated that although Kv2.1 and JPH4 promoted the formation of ER-PMjs, concentrating Kv7.1 in these spots, we could not detect any physical association between the channel and ER-PMj inducers (Figure 7). Thus, Kv7.1 did

not coimmunoprecipitate with either Kv2.1 or JPH4 (Figure 7A). Moreover, FRET efficiency between Kv7.1 and Kv2.1 was low and similar to that under negative conditions (Figure 7B,C). This result suggests that the formation of ER-PMjs is independent of Kv7.1 arrival. Therefore, once these structures are formed, the channel uses these hubs to route toward the plasma membrane. In fact, unlike Kv7.1, Kv2.1 uses the canonical anterograde route to reach the plasma membrane (Figure S6), which could impede their interaction.

Electrophysiology data (Figure 6B) and Kv7.1 surface expression (Figure 3) suggested some differences between Kv2.1- and JPH4-dependent ER-PMjs. In this context, dSTORM was used to analyze the structure and distance between Kv7.1 and ER-PMj inducers in Kv7.1-containing clusters (Figure 8). We expressed Kv7.1 in the presence of KCNE1 (I_{Ks} subunit) and Kv2.1 or JPH4 (ER-PMj inducers). As expected, the colocalization of Kv7.1 with KCNE1 was high, with a close distance between these two proteins (Figure 8B,C). However, colocalization of Kv7.1 with either Kv2.1 or JPH4 was low with larger distances between proteins, which further supported the FRET data. Surprisingly, and in combination with the electrophysiological data, clear differences between Kv2.1- and JPH4-dependent ER-PMjs emerged. Thus, Kv7.1-Kv2.1-containing clusters were more tightly packed than those containing Kv7.1 and JPH4 (Figure 8B,C).

These differences, observed in the electrophysiology and dSTORM studies, were further supported by FRAP analyses. The dynamics of Kv7.1 were different in the presence of Kv2.1. Thus, the mobile fraction of Kv7.1 was higher in the presence of Kv2.1 than when the channel

(A) whole cell — control, +Kv2.1, +JPH4

(B) ER-PMjs — control, +Kv2.1, +JPH4

(C)

	Cells with >2 junctions	ER-PM junctions/cell (mean ± SE)	Maximum junctions per cell	Maximum junctions lenght (µm)
Ø	61% (22/36)	3.84 ± 0.29	7	0.411
Kv7.1	68% (19/28)	4.00 ± 0.32	8	0.574
Kv7.1+Kv2.1	84% (26/31)	10.62 ± 0.67	18	1.390
Kv7.1+JPH4	83% (24/29)	9.96 ± 0.52	16	1.311

(D) Cells with >2 junctions (%) — Ø, Kv7.1, Kv7.1 Kv2.1, Kv7.1 JPH4

(E) ER-PM junctions/cell — Ø, Kv7.1, Kv7.1 Kv2.1, Kv7.1 JPH4

was alone (control) or upon ER-PMjs generated by JPH4 (Figure 9).

To decipher what differences, which differentially alter Kv7.1 function and dynamics, were present in ER-PMjs promoted by Kv2.1 and JPH4, we performed Kv7.1 interactome analysis in HEK 293 cells (Table S1). We refined the data by using the pathway enrichment of Cytoscape software and Reactome databases and the

FIGURE 2 Kv2.1 and JPH4 increased the number and length of ER-PMjs in HEK 293 cells. HEK 293 cells were transfected with Kv7.1-pCDNA3.1 without (control) or with Kv2.1-YFP (+Kv2.1) or JPH4-GFP (+JPH4), and the formation of ER-PMjs was analyzed. (A) Representative electron micrograph showing the ultrastructure of whole cells. Peripheral ER and ER-PMjs are highlighted in different colors. Top panel, Kv7.1-transfected control cells, in green. Center panel, Kv7.1 + Kv2.1 in orange. Bottom panel, Kv7.1 + JPH4 in magenta. Scale bars: 2 μm. (B) Magnifications of ER-PMjs in all conditions. Scale bars: 150 nm. (C–E) Morphometric analysis revealed changes induced by the expression of Kv2.1 and JPH4. HEK 293 cells were not transfected (Ø) or transfected with Kv7.1-pCDNA3.1, without or with Kv2.1-YFP (Kv7.1 + Kv2.1) and JPH4-GFP (Kv7.1 + JPH4). (C) Quantitative morphometric analysis of ER-PMj properties related to number and length. (D) Histogram representation of the number of cells displaying positive ER-PMjs (>2 junctions per cell). The bar graph represents the population in %. (E) Number of junctions per cell studied in the positive group of D. The Bar graph represents the mean ± SE. $^{\ddagger}p < 0.001$ vs. Kv7.1 ($n = 28$–36 cells, Student's t-test).

information available in the UniProtKB/Swiss-Prot database. Thus, two subgroups of proteins (vesicle-mediated traffic and membrane traffic) were further identified (Figure 10, Figures S7 and S8). In agreement with the data in Figure 7, Kv7.1 did not associate with JPH1 (JPH isoform in HEK 293 cells) or, surprisingly, with BIN1 (bridging integrator 1 protein involved in ER-PMjs in skeletal and cardiac muscle[11]) (Figure 10A). However, several proteins from vesicle traffic (Sec22b) and membrane traffic (SORB2, HOMER1, SETP4) coimmunoprecipitated with Kv7.1 (Figure 10B). Since many of these proteins are related to lipid rafts, the presence of Kv7.1 and KCNE1 in these membrane domains was confirmed and subsequently impaired by methyl-β-cyclodextrin (MβCD), a lipid raft disruptor (Figure 10C).

Our data indicated that distinct ER-PMj inducers, such as Kv2.1 and JPHs, influence Kv7.1 function and dynamics. Kv2.1, which also contributes to cardiac currents, and JPHs are essential components of ER-PMjs in striated muscle. Although the contribution of Kv2.1 in generating ER-PMjs in neurons has been addressed,[11,19] its role in muscle has not been elucidated. Kv2.1 participates in neuronal ER-PMjs by interacting with factors such as VAMPs (VAP A and VAP B) and its regulatory subunit AMIGO.[11,15,19] Therefore, we wanted to analyze whether these proteins were differentially involved in Kv7.1-containing ER-PMjs. We expressed Kv7.1 in HEK 293 cells and analyzed the interaction with endogenous VAP A, VAP B, and AMIGO in the presence of either Kv2.1 or JPH4 (Figure 11). Interestingly, Kv7.1 was associated with VAP A, VAP B, and AMIGO (Figure 11A). These associations were not a consequence of Kv7.1 overexpression, according to the negative co-IP results with other related proteins provided in Figures 7 and 10A. Thus, to our knowledge, these data showed for the first time that VAMPs and AMIGO, binding partners of Kv2.1, interacted with Kv7.1, suggesting similar spatial localization by both channels. In addition, co-IP experiments showed that VAP B was more abundant in Kv7.1 co-IPs in the presence of Kv2.1. These data suggest that a differential ER-PMj protein composition and interaction fine-tune the function and dynamics of the cardiac Kv7.1 channel.

3 | DISCUSSION

The voltage-dependent K⁺ channel Kv7.1 associates with the KCNE1 β-regulatory subunit to generate the cardiac I_{Ks} current.[1,2] This K⁺ current is crucial for the termination of cardiac action potentials. The association takes place in ER-PMjs before translocation to the plasma membrane.[7,8] Thus, the I_{Ks} channel, expressed in the sarcolemma as well as its contact sites with the SR, is located in the characteristic T-tubule structures, which house the ion channel machinery for excitation-contraction (E-C) coupling. T-tubules have many RyR and LTCCs, which contribute to the regulation of cellular calcium.[11] A major issue surrounding the Kv7.1-KCNE1 associate includes the anterograde route of Kv7.1-KCNE1 to the plasma membrane as well as the cellular compartment where association takes place. Two major lines of evidence have been reported: (i) the association takes place early in the ER, and (ii) the interaction dynamically occurs at the plasma membrane.[7–10] Recent findings indicate that Kv7.1 and KCNE1 travel to the cell membrane using different routes, thereby associating late in the biogenesis of ER-PMjs before delivery to the cell surface.[7] Indeed, this claim would merge both hypotheses and support the localization of the complex at the cardiac sarcolemma and T-tubules as widely described.

Unlike KCNE1, Kv7.1 is unconventionally transported to the plasma membrane via ER-PMjs.[7,8] Therefore, we investigated the route and Kv7-1-related inducers of ER-PMjs, which govern the expression of the channel at the cell surface. Our work describes that Kv2.1, a neuronal K⁺ channel that also contributes to cardiac action potentials, and JPHs, facilitate the formation of ER-PMjs and upregulate the expression and function of Kv7.1 at the HEK 293 cell membrane and AC16 human cardiomyocytes. The legitimacy of HEK 293 cells for these studies – probably due to their neuronal fetal kidney origin[21]– has been soundly validated by the recapitulation of conformational coupling of Cav1.1 and RyR1 in HEK 293 cells transiently transfected with RyR1, Cav1.1, STAC3, Cavβ1a, and JPH2.[22]

Our data showed that Kv2.1, which is implicated in neuronal ER-PMjs, is effective in localizing Kv7.1 in these structures. Although migrating by different mechanisms
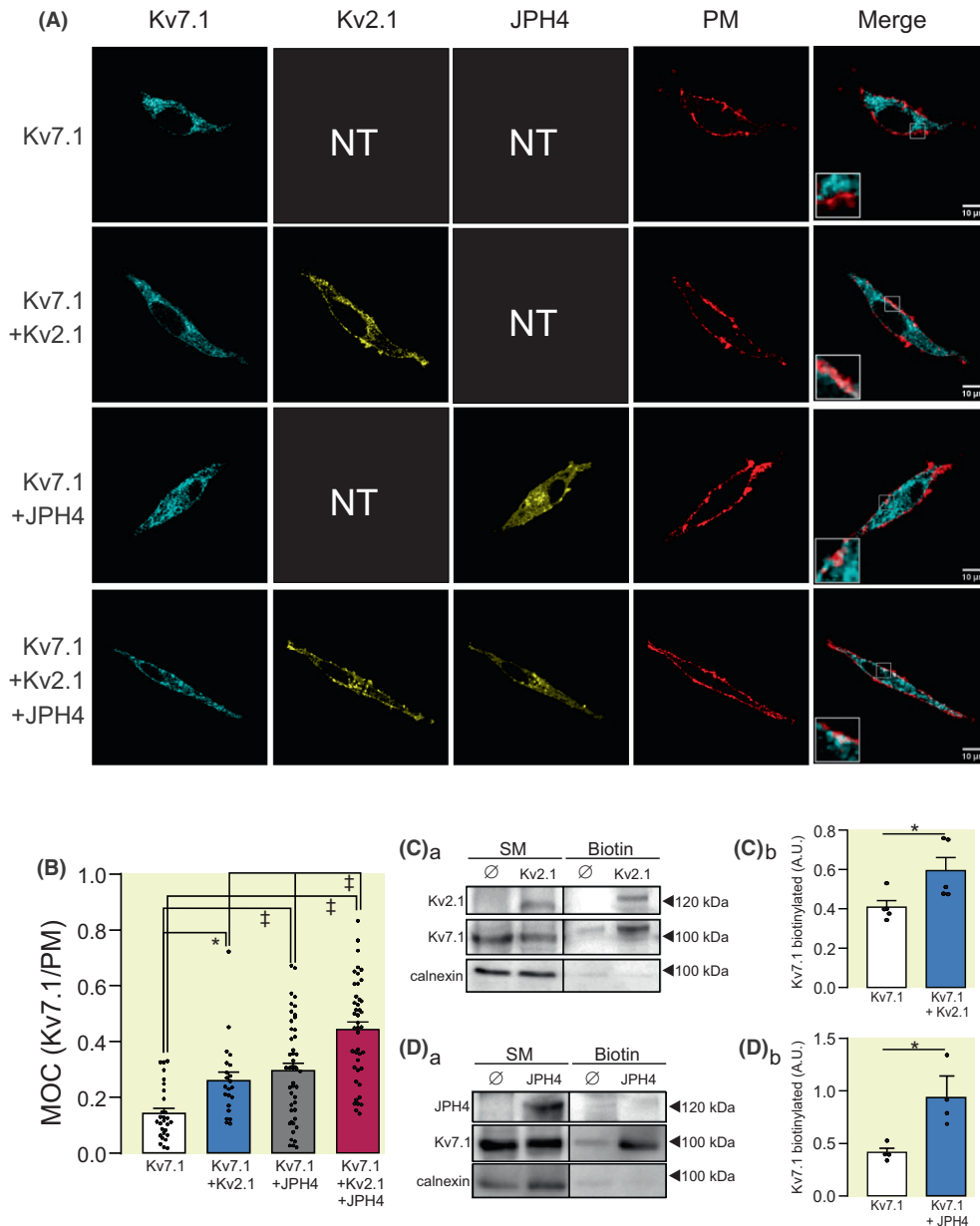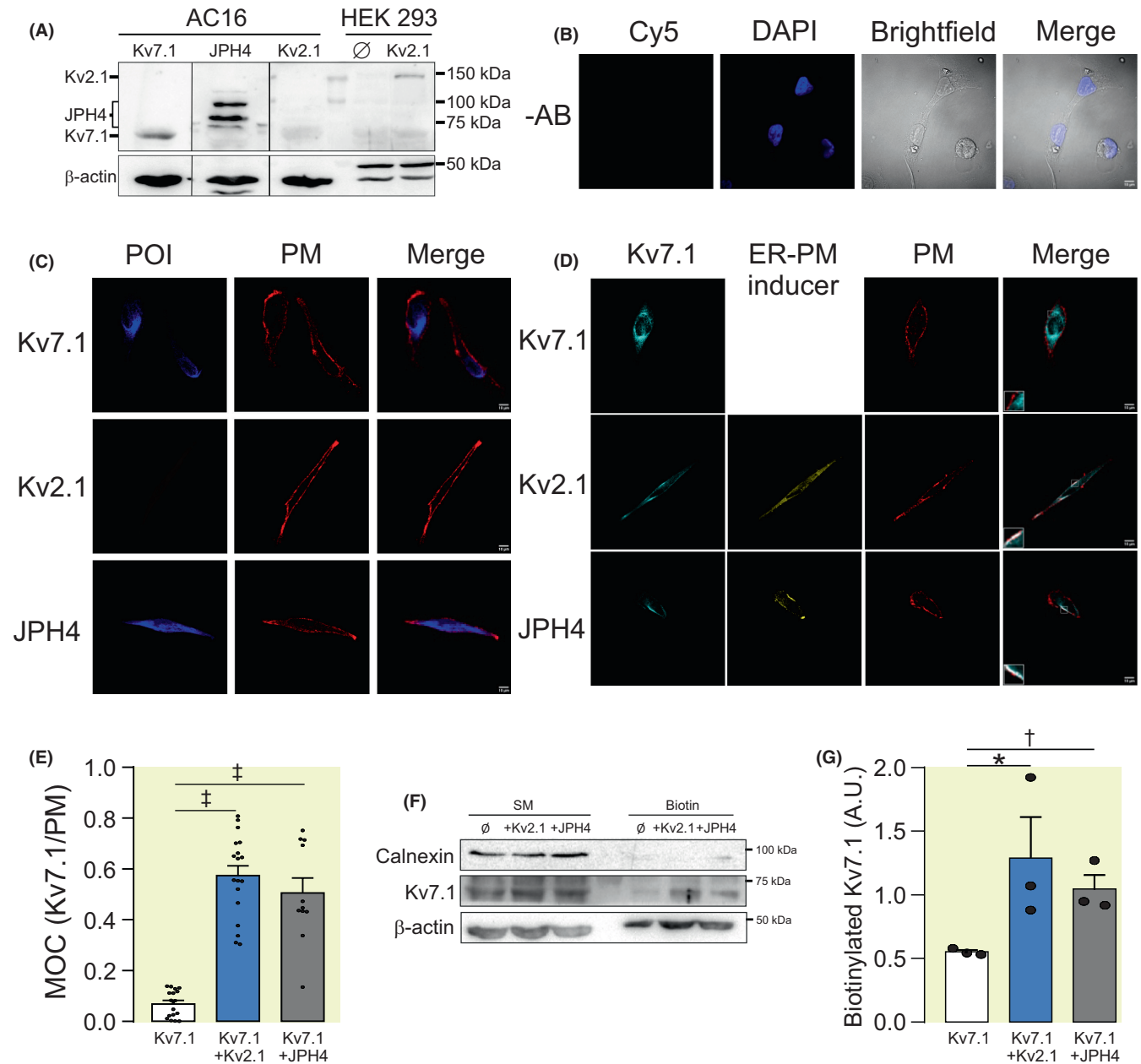
FIGURE 3 Kv2.1 and JPH4 enhance Kv7.1 plasma membrane targeting in HEK 293 cells. HEK 293 cells were transfected with Kv7.1-CFP with or without Kv2.1-YFP and JPH4-GFP, and the expression of Kv7.1 at the cell surface was analyzed. (A) Representative confocal microscopy images. Kv7.1-CFP (blue); ERPMj inducers Kv2.1-YFP and JPH4-GFP (yellow); the PM marker Akt-PH-pDsRed (red). Merge shows colocalization between Kv7.1 and PM marker in white. Insets zoom selected areas. Scale bar, $10\,\mu m$. NT, no fluorescence was observed when the specific protein was non-transfected. (B) Manders' overlapping coefficient (MOC) analysis of Kv7.1 overlapping PM marker 48 h after transfection in different conditions (Kv7.1 alone, Kv7.1 + Kv2.1, Kv7.1 + JPH4 and Kv7.1 + Kv2.1 + JPH4). The bar graph represents the mean $\pm$ SE. $*p < 0.05$, $^{\ddagger}p < 0.001$, (Student's t-test). (C and D) Protein biotinylation assays. HEK 293 cells were transfected with Kv7.1-CFP without (Ø) or with Kv2.1-YFP (C) and JPH4-GFP (D). After 48 h of transfection, cells were labeled with biotin to detect plasma membrane proteins and processed as described in Materials and Methods. (Ca and Da) representative filters; (Cb and Db) quantification of 4–6 independent experiments. The bar graph represents the mean $\pm$ SE. $*p < 0.05$ (Student's t-test). Calnexin was used as a negative control. SM: starting materials; Biotin: pull down of biotinylated proteins.

to the plasma membrane, both channels contribute to cardiac action potentials. Therefore, their commonalities, not only in activity but also in spatial location, deserve attention. In fact, we found that VAMPs, such as VAP A and VAP B, and AMIGO, a Kv2.1 interacting protein, were associated with Kv7.1. These results situate these adaptors, which are important players that facilitate ER-PMjs, as major scaffolds in Kv7.1 localization in ER-PMjs.

Nonconducting neuronal Kv2.1 channels form clusters – corrals – that act as traffic hubs for other proteins

FIGURE 4 Kv2.1 and JPH4 enhance Kv7.1 plasma membrane targeting in AC16 cardiomyocytes. Human AC16 cells were transfected with or without Kv2.1-YFP and JPH4-GFP, and the endogenous expression of Kv7.1 at the cell surface was analyzed. (A) AC16 cells express endogenous Kv7.1 and JPH4, but not Kv2.1. HEK 293 cells were transfected with (Kv2.1) or without (Ø) Kv2.1-YFP and filters immunoblotted against Kv2.1 for control. (B) Representative confocal microscopy images in the absence of primary antibodies (-AB) demonstrating the specificity of the endogenous Kv7.1, JPH4, and Kv2.1 staining. Cy5 secondary antibody in the absence of Kv7.1 antibody; DAPI, nuclei staining; Bright-field microscopy; Merge of all channels. The scale bar represents 10 μm. (C) Representative confocal microscopy images of endogenous protein of interest (POI, blue). PM marker (WGA staining, red). Merge shows colocalization between Kv7.1 and PM marker, in magenta. Scale bar, 10 μm. (D) Confocal microscopy images of endogenous Kv7.1 expression (blue) in AC16 transfected without or with Kv2.1-YFP or JPH4-GFP (ER-PM inducer, yellow). PM marker (WGA staining, red). Merge shows colocalization between Kv7.1 and PM marker, in white. Insets zoom selected areas. Scale bar, 10 μm. (E) Manders' overlapping coefficient (MOC) analysis of Kv7.1 overlapping PM marker 48 h after transfection in different conditions (Kv7.1 alone, Kv7.1 + Kv2.1 and Kv7.1 + JPH4). The bar graph represents the mean ± SE. $^{‡}p < 0.001$ (Student's t-test). (F and G) Protein biotinylation assays. AC16 cardiomyocytes were transfected without (Ø) or with Kv2.1-YFP or JPH4-GFP. After 24 h of transfection, cells were labeled with biotin to detect plasma membrane proteins and processed as described in Materials and Methods. (F) Representative filters. (G) Quantification of 3 independent experiments. The bar graph represents the mean ± SE. $^{*}p < 0.05$, $^{†}p < 0.01$ (Student's t-test). Calnexin was used as a negative control. SM: starting materials; Biotin: pull down of biotinylated proteins.
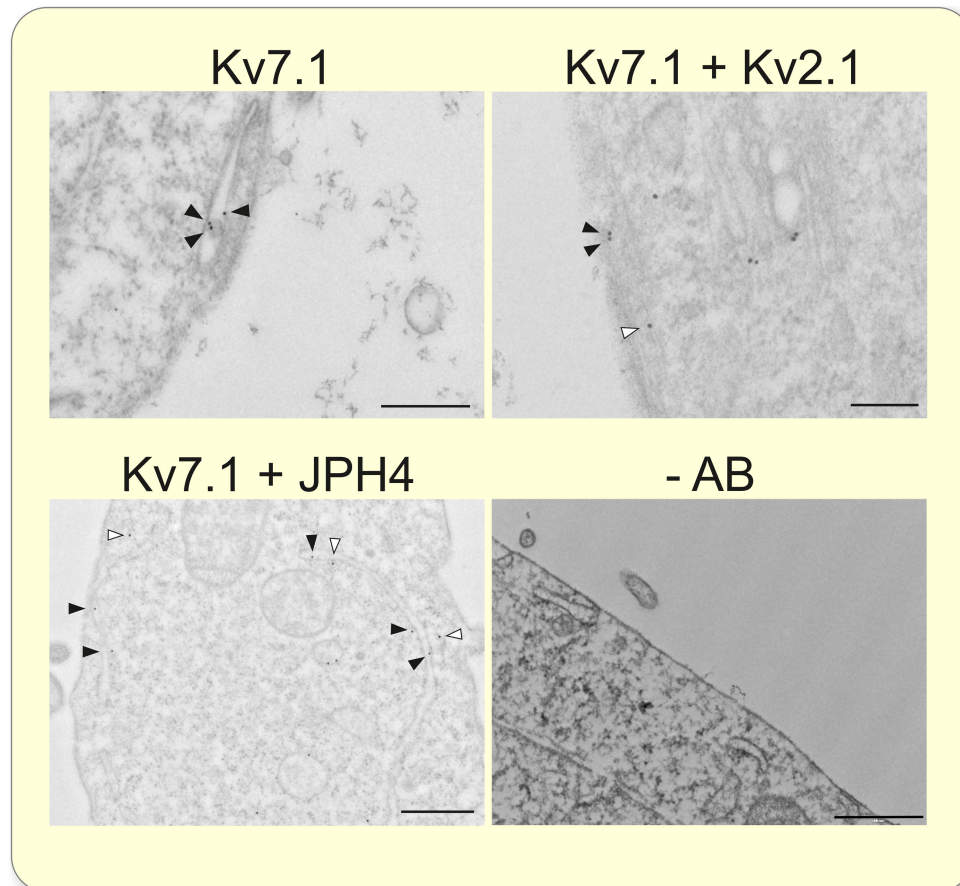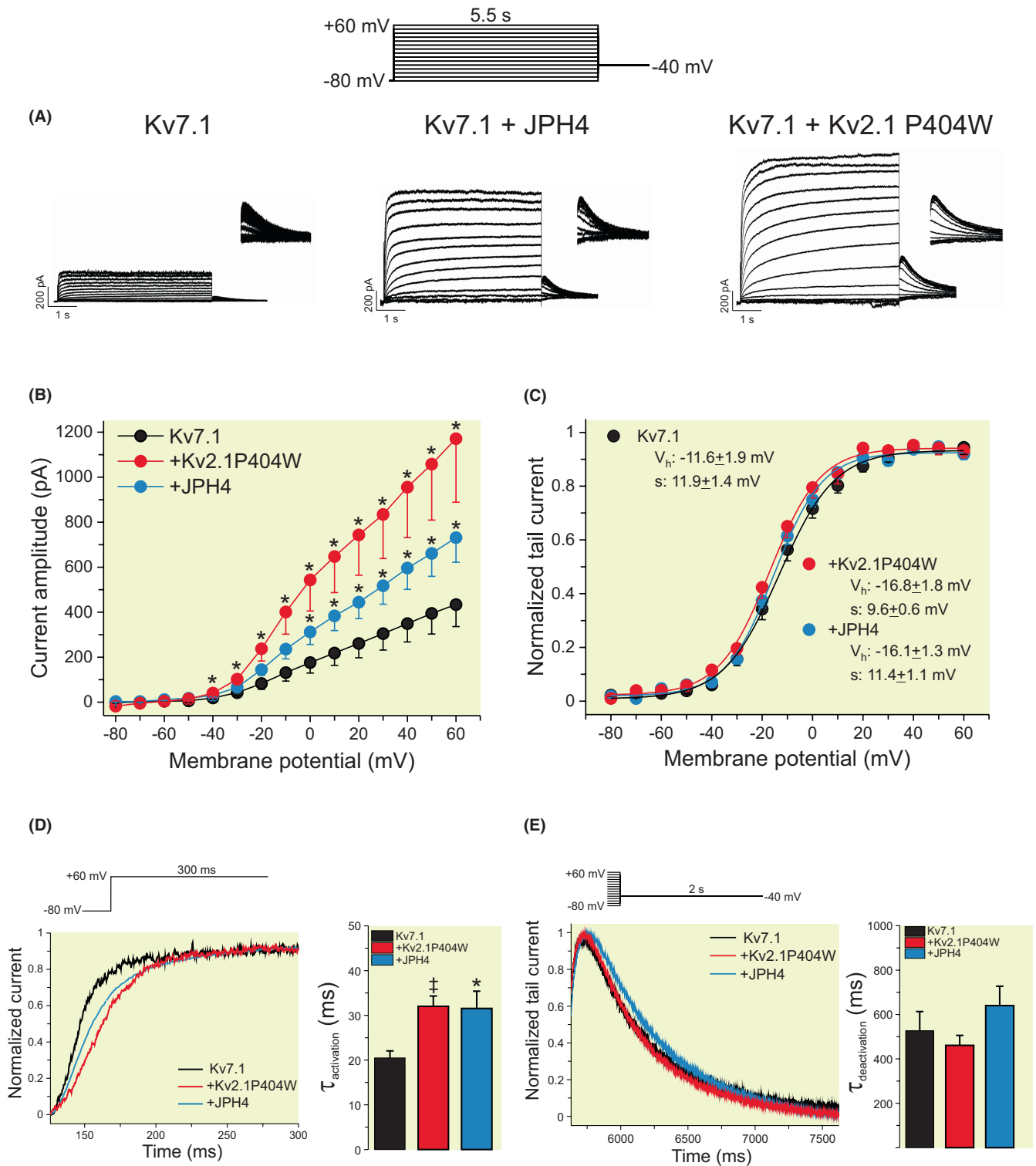
FIGURE 5 Kv7.1 targeted ER-PMjs. HEK 293 cells were transfected with Kv7.1-pCDNA3.1 without Kv7.1 or with Kv2.1-YFP (Kv7.1 + Kv2.1) or JPH4-GFP (Kv7.1 + JPH4). Kv7.1 (black arrowheads) targeted to ER-PMjs and peripheral ER in all conditions. Kv2.1 and JPH4 (white arrowheads) were used to label specific ER-PMjs generated by these ER-PMj inducers. Scale bars: 150 nm. While Kv7.1 was stained with 12 nm gold particles, 18 nm gold particles stained Kv2.1-YFP or JPH4-GFP. −AB, negative control in the absence of primary antibodies.

to reach these specific membrane domains.[23] To date, Kv2.1 has not been linked to the formation of ER-PMjs in the heart. Our data suggested that Kv2.1, in addition to its function as an ion channel, has a potential role in cardiac architecture. Moreover, JPHs are crucial for the generation of dyads in cardiomyocytes, neuronal signaling, and activation of T cells.[11,24] While JPH1-2 are cardiac isoforms, JPH3-4 are expressed in the brain. Normally, JPH1-2 requires the presence of other proteins to generate these ER-PMjs (e.g., JPH2 and Cav1.2), whereas JPH4, the isoform studied in this work, generates contacts between the ER and the PM by itself.[11]

Despite the origin, the ER-PMj membrane morphology was similar in all conditions. In many of the experiments, the extension of the ER was close to the PM until reaching distances inferior to 20 nm. JPH4 and Kv2.1 formed thin dense hooks that perpendicularly attached the ER to the PM and shaped Kv7.1 annular formations, previously described as donut-like structures.[19] These structures match precisely with the morphology generated by

JPH4 and other proteins, such as the STIM-ORAI complex, RyR, or synaptogamines.[22,25,26] In fact, dynamic ring-shaped ER-PM contact sites change the morphology of the junctions in response to reticular calcium movements.[27] For example, the STIM1 puncta signal reshapes into annular structures when extended synaptogamines (E-syt) relocate to the central area of these microdomains. Interestingly, E-syt1 alone induces these ring-shaped contacts; in contrast, STIM1 by itself can only generate the classical ER-PMjs clusters.[28] Moreover, distances between the ER and the PM were different depending on the protein involved. This finding suggests that different proteins generate different types of ER-PMjs, morphologically and functionally, as both promote different calcium responses. Our results showed that Kv7.1 was also found in the ring-shaped ER-PMjs, assembling with KCNE1 to generate the I_{Ks} complexes.

In this context, synaptogamines, suspected to be involved in the formation of these structures, were not detected in the Kv7.1 interactome in HEK 293 cells.

FIGURE 6 Kv2.1 and JPH differentially affected the electrophysiological characteristics of Kv7.1. COS-7 cells were transfected with Kv7.1-pCDNA3.1 without Kv7.1 or with Kv2.1-YFP (Kv7.1 + Kv2.1 P404 W) or JPH4-GFP (Kv7.1 + JPH4). K^+ currents were elicited using patch-clamp configuration following the indicated protocol 48 h after transfection. Nonfunctional Kv2.1P404 W-YFP was used to avoid current interference. (A) Representative traces and tail currents. (B) Current amplitude vs. membrane potential plot. *$p < 0.05$ vs. Kv7.1 ($n > 10$ cells, Student's t-test). (C) Normalized tail currents vs. membrane potential plots. No differences in V_{half} activation (V_h) or slope (s) were found among the groups. (D) Normalized peak current at +60 mV vs. time plot. Left panel, representative traces following the described protocol. Right panel, τ of current activation. (E) Representative normalized tail currents were elicited following the described protocol. Left panel, representative traces. Right panel, τ of deactivation. Black traces and bars, Kv7.1 alone; red traces and bars, Kv7.1+ Kv2.1P404 W; blue traces and bars, Kv7.1 + JPH4. Values are presented as the mean + SE. *$p < 0.05$; ‡$p < 0.001$ vs. Kv7.1 alone ($n > 20$ cells per condition, Student's t-test).
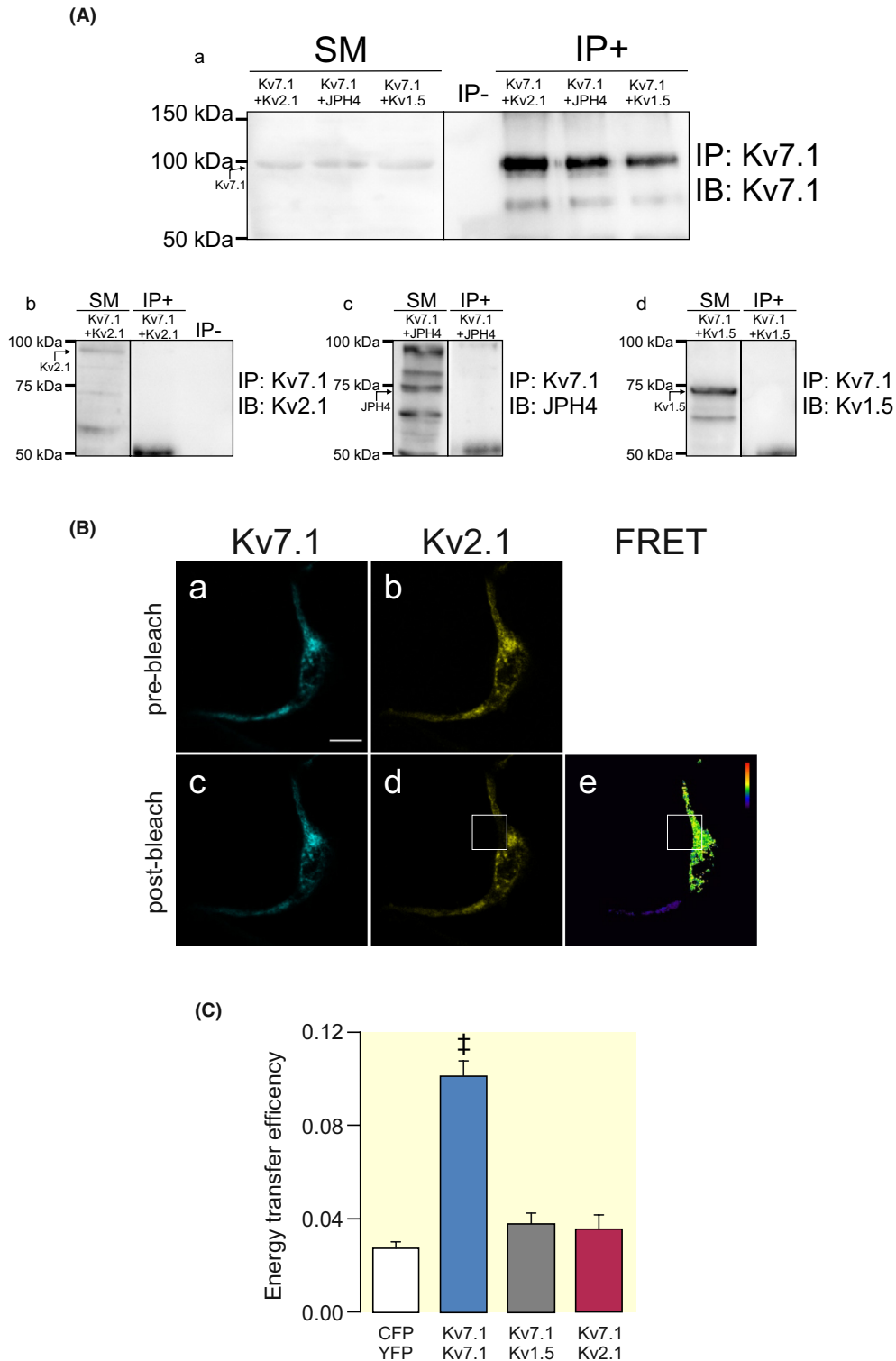
FIGURE 7 Kv7.1 did not interact with either Kv2.1 or JPH4. HEK 293 cells were cotransfected with Kv7.1-CFP and Kv2.1 or JPH4. Kv1.5 was also transfected and used as a negative control. (A) Total lysates were obtained from cells after 48 h of transfection, and proteins were immunoprecipitated (IP) with an anti-GFP antibody. Immunoprecipitates were immunoblotted (IB) against Kv7.1-CFP (a), Kv2.1 (b), JPH4 (c), and Kv1.5 (d). IP+, immunoprecipitate; IP−, immunoprecipitation in the absence of anti-CFP antibody; SM, starting material. (B and C) FRET experiments between Kv7.1-CFP and Kv2.1-YFP. (Ba, b) Prebleaching images of Kv7.1 in cyan and Kv2.1 in yellow. (Bc–e) Postbleaching images of Kv7.1 in cyan and Kv2.1 in yellow. The bleached area is highlighted by a white square. (Be) FRET ratio image. Calibration bars indicate FRET ratios ranging from 0.6 (blue) to 1.7 (red). Scale bar: 10 μm. (C) Energy transfer efficiencies. While Kv7.1-CFP and Kv7.1-YFP were used for positive tetramerization, Kv7.1-CFP and Kv1.5-YFP denoted negative interactions. Values represent the mean ± SE. $^{\ddagger}p < 0.001$ vs. CFP-YFP negative control ($n = 10$–24 cells, Student's t-test).
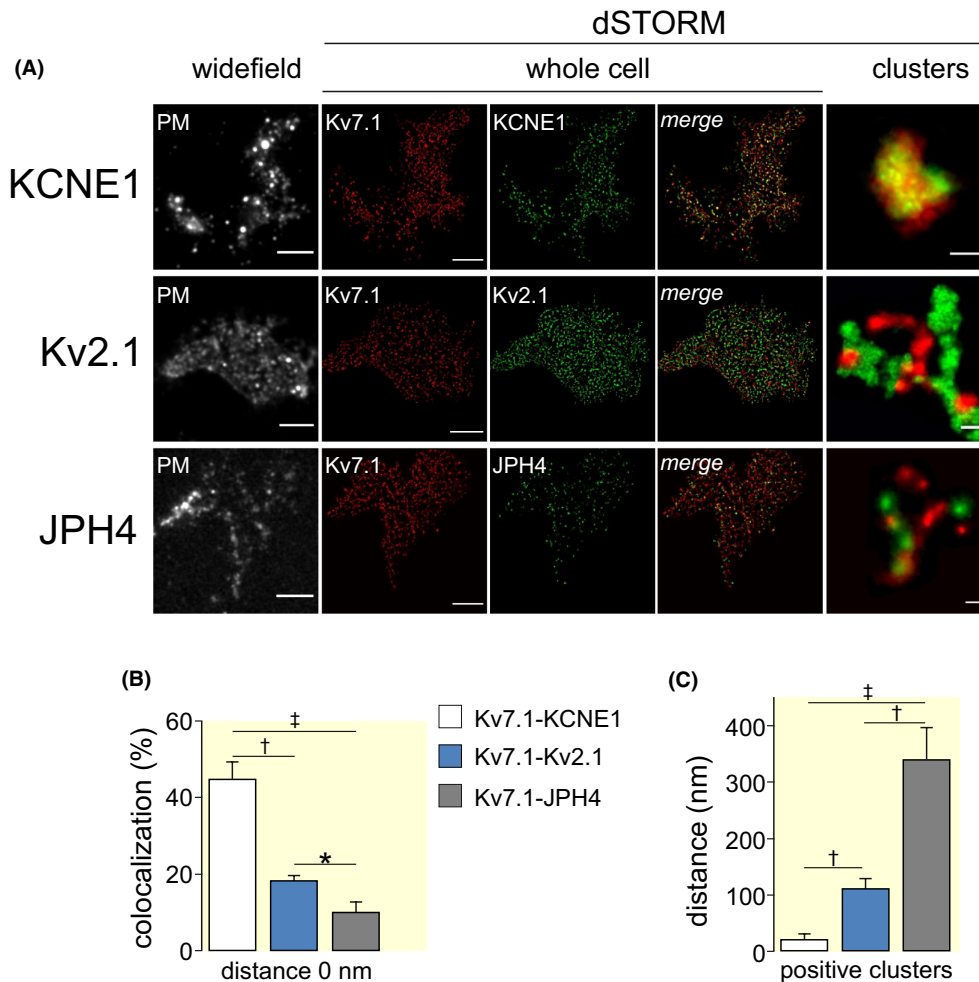
FIGURE 8 Proximity between proteins in ER-PMjs assessed by dSTORM. HEK 293 cells were transfected with Kv7.1-CFP and KCNE1-YFP, Kv2.1-YFP, or JPH4-GFP and coexpressed with Akt-PH-pDsRed (PM marker). (A) mCUPs were isolated and immunolabeled with specific antibodies for superresolution imaging 48 h after transfection. The PM marker was observed by widefield microscopy and used to delineate cells. Dual color direct stochastic optical reconstruction microscopy (dSTORM) was then performed in whole cells and ER-PMj clusters. Representative superresolution images are shown. Kv7.1, in red; KCNE1, Kv2.1, and JPH4 appear in green. Merged images of total cells and clusters showed colocalization in yellow. Scale bar, 5 μm. (B) Colocalization at a distance of 0 nm was determined by dSTORM analysis. Distances were calculated between Kv7.1 and the other proteins in each condition (Kv7.1-KCNE1, white bars; Kv7.1-Kv2.1, black bars; Kv7.1-JPH4, gray bars). Values represent the mean ± SE of all paired single-molecule localizations from each cell. $*p < 0.05$, $^{\dagger}p < 0.01$ and $^{\ddagger}p < 0.001$ ($n = 4$–5 cells; Student's t-test). (C) The mean distance between proteins in positive clusters. Distances were calculated between Kv7.1 and the other protein in each condition (Kv7.1-KCNE1, white bars; Kv7.1-Kv2.1, blue bars; Kv7.1-JPH4, gray bars). Values represent the mean ± SE. $^{\dagger}p < 0.01$ and $^{\ddagger}p < 0.001$ ($n = 4$–5 cells; Student's t-test).

Therefore, other proteins might be involved in the reshaping of these contact sites, facilitating the formation of annular structures. Moreover, with no interaction, Kv7.1 and Kv2.1 are closer than Kv7.1 and JPH4. This finding suggests that some components of Kv2.1-related ER-PMjs are more tightly associated with Kv7.1 than those present in JPH4-related ER-PMjs. Our studies indicated that Kv7.1 and Kv2.1 share, at least, interactions with VAPMs and AMIGO. Both scaffolding groups of proteins are Kv2.1 partners that contribute to ER-PMj formation.[15] In fact, from our data, VAP B is more abundant in Kv2.1-related ER-PMjs than in those containing JPH4.

In addition, we examined other Kv7.1 interactors participating in the localization of Kv7.1 ER-PMjs in HEK 293 cells. Neither JPH1, which is the isoform expressed in HEK 293 cells, nor BIN1 (amphiphysin II/bridging integrator 1 protein), which contributes to the trafficking of Cav1.2 to the dyads in cardiomyocytes,[11] interacted with Kv7.1. While few COPII-related proteins were found (Sec22b), many proteins of the COPI coatomer were detected (COPa, COPb, COPd, COPe, or ARF4), suggesting that while little Kv7.1 escapes the ER, there is consistent control machinery ensuring that the channel is returned to the ER, avoiding the Golgi.[29] Furthermore, few proteins
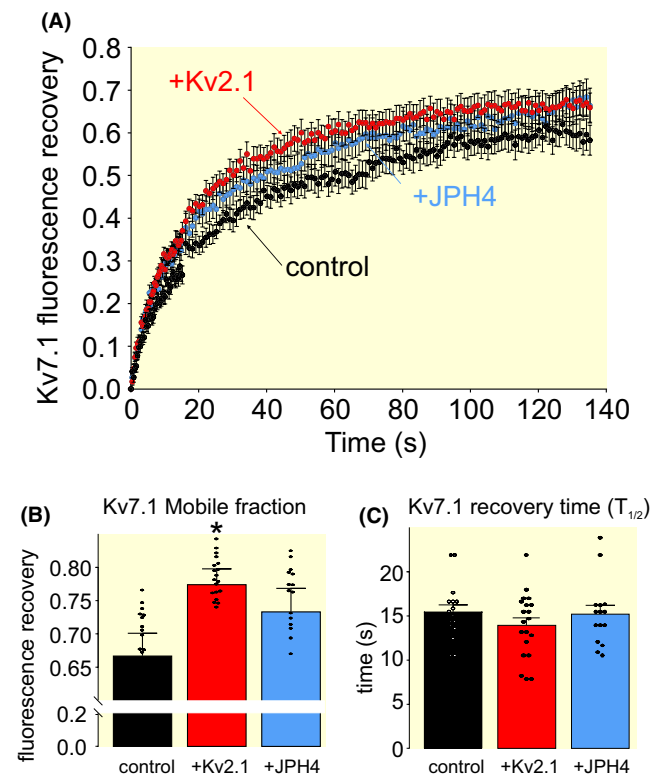
FIGURE 9 Kv7.1 dynamics in the presence of Kv2.1 and JPH4. FRAP performed 48 h after Kv7.1-CFP transfection in HEK 293 cells without (control) or with Kv2.1 (+Kv2.1-YFP) and JPH4 (+JPH4-GFP). (A) Fluorescence recovery over time. (B) Mobile fraction. (C) Kv7.1 half-live recovery. Black symbols and bars, control (Kv7.1 alone); red symbols and bars, Kv7.1 + Kv2.1; blue symbols and bars, Kv7.1 + JPH4. Values are presented as the mean ± SE, $n > 10$ cells. *$p < 0.05$ vs. control (Student's t-test).

related to intra-Golgi transport, such as ADP-ribosylation factor-like protein 1 (ARL1) or the vesicular-fusion protein NSF and trans-Golgi network vesicle budding (clathrin light chain A [CLTA] and ARF1), which are related to clathrin-mediated transport or endocytosis mechanisms independent of Golgi exit, were found in the Kv7.1 interactome. In addition, we found several lipid raft-related proteins supporting the raft-enriched ER-PMj localization of Kv7.1 as well as the role of ER-PMjs in lipid transportation.[30]

Kv2.1 and JPH4 affected the number and length of the complex, but Kv7.1 generated no effects on ER-PMj morphology. Therefore, unlike Kv2.1 and JPH4, the channel traveled to already formed hubs. Data also supported that Kv7.1, with no interaction with Kv2.1 or JPH4, uses three types of ER-PM junctions: (i) "native" or endogenous, (ii) those generated by Kv2.1 and (iii) those promoted by JPH4. In fact, colocalization analysis of Kv2.1 with post-ER subcellular compartments indicated that this channel, similar to KCNE1 and unlike Kv7.1, followed the classical secretory pathway. These results suggested that ER-PMj

inducers do not need ER-PMjs as a traffic mechanism to reach the membrane. Kv2.1 appears to facilitate the formation of junctions once it reaches the membrane. Once there, these clusters hub other proteins, such as Kv7.1, to access the cell surface. In addition, the architecture of ER-PMjs varies because the distances between Kv7.1 and Kv2.1 or JPH4 and the membrane dynamics of Kv7.1 are different.

From our data, we conclude that the relationship between Kv2.1 and JPH4 with Kv7.1 is not the same. JPH4 generates contacts between the ER and the PM for Kv7.1, which is used as a mechanism for reaching the membrane. Once there, the channel diffuses along the membrane and the junctions and, thus, interacts with junctophilin. Kv2.1, instead, could not only generate the contacts used for trafficking but also trap Kv7.1 channels, share binding partners, and alter channel dynamics. The relationship between Kv7.1 and Kv2.1 encompasses more than just migration. Kv2.1 and JPHs are also both involved in the formation of dyadic structures. JPHs attach the ER to the phospholipids of the PM to stably anchor both membranes. Due to alpha helix domains located in the medial domain of the molecule, JPHs are elastic and regulate the dyad/ER-PM junction distance. Direct association with calcium channels from the PM and the SR has been described, in addition to their anchoring function. Moreover, these associations stabilize and modify the gating and current properties of both LTCC channels and RyR.[11]

To what extent the protein composition and architecture may affect Kv7.1 function, thereby shaping cardiac action potentials, is intriguing. However, our data indicate that, at least, the current density and channel dynamics are affected. In fact, studies in other excitable cells have exposed similarities but also important cell type–specific differences in the structure and function of ER-PMjs that surely remodel the fate of the ion channels.

4 | MATERIALS AND METHODS

4.1 | Plasmids, mutagenesis, and transient transfection

The genetic materials were sourced from various institutions and individuals. T. Jentsch (Leibniz-Institut für Molekulare Pharmakologie and Max-Delbrück-Centrum für Molekulare Medizin, Germany) provided the hKv7.1 complementary DNA (cDNA) in a pTLN vector. S. de la Luna (Centro de Regulación Genómica, Spain) contributed the hKCNE1 cDNA in a pHA vector. M. Tamkun (Colorado State University, USA) supplied YFP-rKv2.1HA and JPH4-GFP. To confocal microscopy and molecular biology studies, cDNAs of Kv7.1, KCNE1, Kv2.1, JPH4,
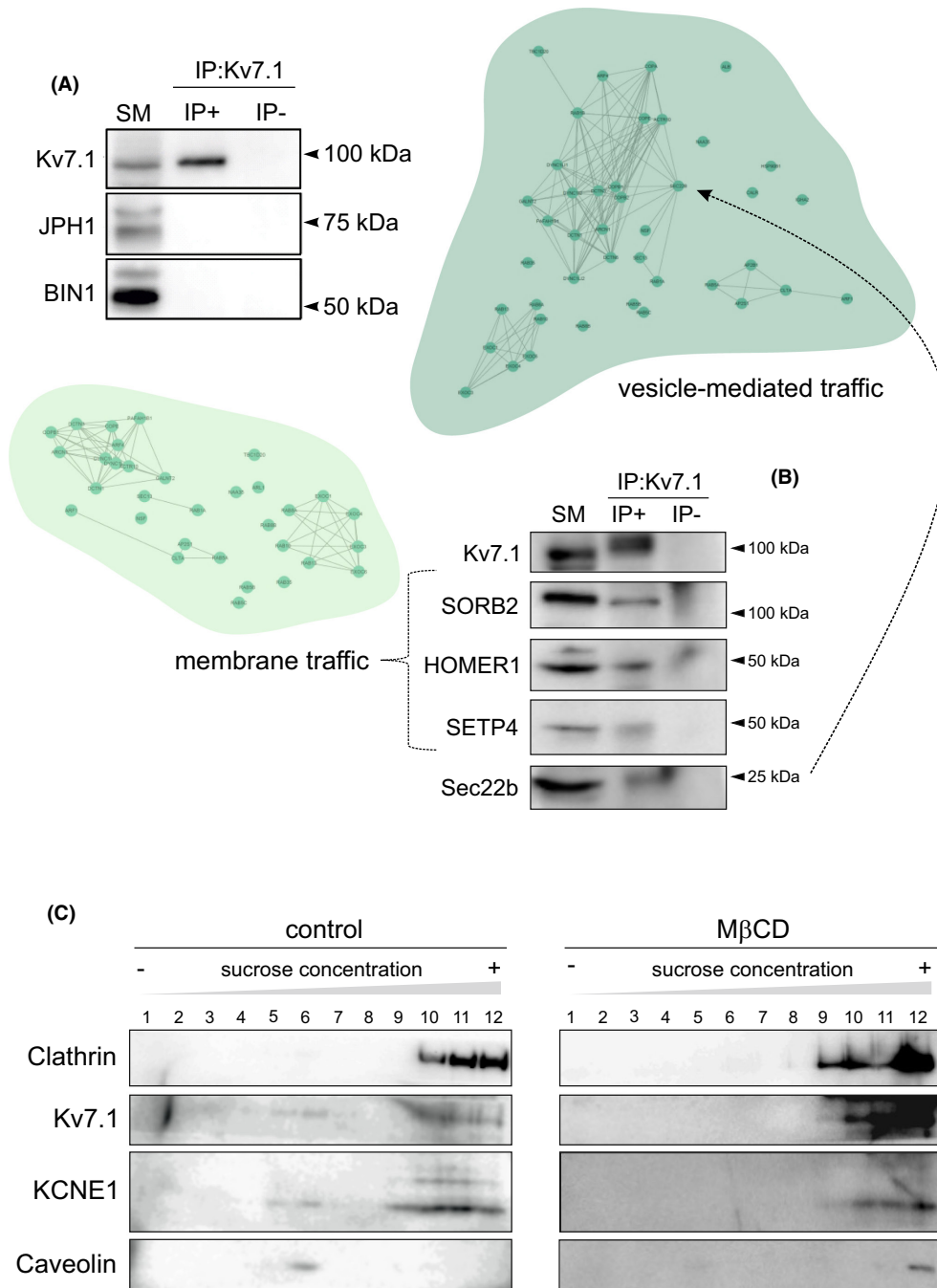
FIGURE 10 Deciphering Kv7.1 interactions. HEK 293 cells were transfected for 48 h with Kv7.1-CFP, and channel interactions and interactomes were analyzed. (A) Coimmunoprecipitation of Kv7.1 using an anti-Kv7.1 antibody (IP: Kv7.1) in whole cell lysates from HEK 293 cells transfected with Kv7.1-CFP. The top panel, immunoblotting against Kv7.1; the center panel, JPH1; the bottom panel, immunoblotting against BIN1. IP+, immunoprecipitates; IP−, immunoprecipitation in the absence of anti-Kv7.1 antibody; SM, starting material. (B) Representation of two Kv7.1 interactome networks obtained by mass spectrometry. Pathways were established using Cytoscape software and Reactome databases and tagged in the graphic with colors to distinguish the networks involved in the membrane (light green shape) and vesicle-mediated (dark green shape) migration. Interactors were classified by using pathway enrichment software and the information available in the UniProtKB/Swiss-Prot database. Green circles show interactors, and interactions appear as gray lines forming the networks. Bottom panel, coimmunoprecipitation of Kv7.1 with selected interactors. Whole-cell lysates from HEK 293 cells transfected with Kv7.1-CFP were coimmunoprecipitated using an anti-Kv7.1 antibody (IP: Kv7.1) and immunoblotted against specific proteins (SORB2, HOMER1, SETP4, Sec22b). IP+, immunoprecipitate; IP−, immunoprecipitation in the absence of anti-Kv7.1 antibody; SM, starting material. (C) Lipid raft microdomain isolation. Representative sucrose density gradients of extracts from HEK 293 cells transfected with Kv7.1-CFP and KCNE1-YFP (used as a control). Cells were treated without (control) or with (MβCD) methyl β cyclo-dextrin as indicated in the Materials and Methods to disrupt raft domains. While caveolin indicates low-buoyancy rafts, clathrin is distributed in nonfloating fractions. Numbers denote different fractions from the top (1) to the bottom (12) of the sucrose density gradient. Samples were immunoblotted against Kv7.1, KCNE1, caveolin, and clathrin.
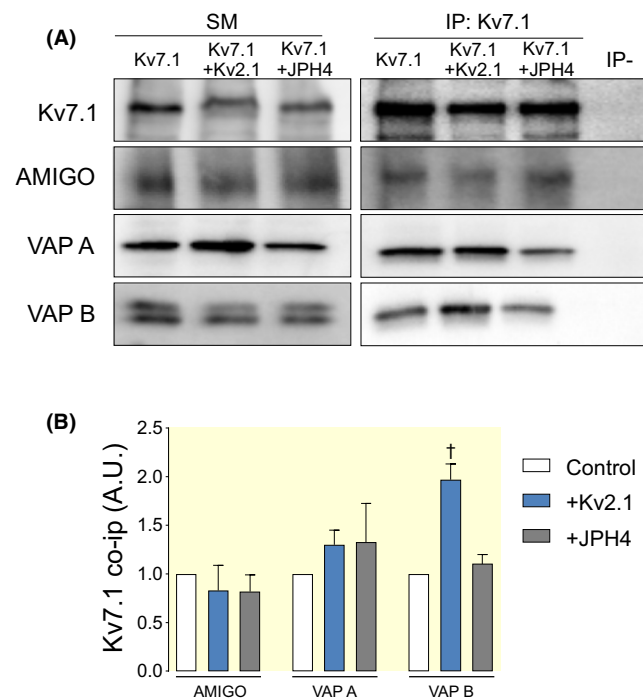
and Kv1.5 were incorporated into pECFP-N1, pEYFP-N1, and pEYFP-C1 vectors (Clontech). Modification of the Kv2.1 channel was executed through mutagenesis to obtain a nonfunctional channel (Kv2.1 P404 W) utilizing the QuikChange multisite-directed mutagenesis kit (Agilent Technologies). All constructed materials were verified through sequencing. In addition, the PDsRed-tagged pleckstrin homology (PH) domain of Akt (Akt-PH-pDsRed), used as a membrane marker, was generously provided by F. Viana (Universidad Miguel Hernández, Spain) while the ER marker (pDsRed-ER), pECFP-N1, and pEYFP-N1 were acquired from Clontech.

4.2 | Cell culture

Human AC16 cardiomyocytes, HEK 293, and COS-7 cells were cultured in Dulbecco's modified Eagle's medium supplemented with 10% (v/v) fetal bovine serum (FBS)

FIGURE 11 Kv2.1 binding partners promoted the formation of ER-PMjs and interacted with Kv7.1. HEK 293 cells were transfected with Kv7.1-CFP alone or together with Kv2.1-YFP or JPH4-GFP. After 48 h of transfection, total lysates were immunoprecipitated against Kv7.1 (IP: Kv7.1), and samples were immunoblotted (IB) against Kv7.1, AMIGO, VAP A, and VAP B. (A) Representative Western blots. IP−, immunoprecipitation in the absence of anti-Kv7.1 antibody; SM, starting material. (B) Relative quantification of protein abundance coimmunoprecipitation from Kv7.1 immunoprecipitates in Panel A. Values are presented as the mean $\pm$ SE ($n=4$–6). †$p<0.01$ vs. control (Kv7.1 alone) Student's t-test. White bars, Kv7.1 alone (control no additions); blue bars, Kv7.1 + Kv2.1; gray bars, Kv7.1 + JPH4.

and penicillin/streptomycin (100 U/mL). The culture media for AC16 cells was tailored, comprising 12.5% (v/v) FBS, 2 mM L-Glutamine, and penicillin/streptomycin (100 U/mL). Experimental setups involving molecular biology were conducted with cells seeded in 100-mm culture dishes. For confocal microscopy, cells were seeded onto poly-d-lysine–coated coverslips. Transient transfection protocols utilized Lipotransfectine (AttendBio Research) once cells achieved approximately 80% confluence. Certain experiments involved BFA (Sigma–Aldrich) at a concentration of 5 μg/mL for 4 h to ensure the complete turnover of Kv7.1 and Kv7.1-KCNE1 complexes. In some experiments, cells were cultured for 20 min with 10 mM methyl-β-cyclodextrin (MβCD) prior to protein extraction.

In transwell permeable support experiments, HEK 293 cells were cultured in permeable polyethylene terephthalate (PET) supports with a 0.4 μm pore (Transwells®, Costar). To avoid osmotic interference, the medium was always changed in the following order: empty basolateral chamber, empty apical chamber, fill the apical chamber, fill the basolateral chamber. Cell culture and transfection protocols were then applied following the same procedures as previously explained. For immunocytochemistry, the microporous membrane was cut using a scalpel. This membrane was mounted on a slide, with the cells facing up, and then covered with a coverslip. Special attention was given to not compress the cells to maintain their volume and cell morphology.

4.3 | Cell unroofing preparations (CUPs) and immunocytochemistry

CUPs, identified as membrane sheets, were acquired by subjecting cells to osmotic shock.[7] HEK 293 cells were seeded on poly-d-lysine–treated glass coverslips. Forty-eight hours after transfection, the cells were cooled on ice for 5 min and washed twice in phosphate-buffered saline (PBS). Subsequently, a 5-min incubation in KHMgE buffer [70 mM KCl, 30 mM HEPES, 5 mM MgCl$_2$, and 3 mM EGTA (pH 7.5)] was conducted, followed by a three-fold dilution and gentle washing with undiluted KHMgE to induce hypotonic shock. The lysed cells were then eliminated from the coverslips through pipetting. After two additional washes with KHMgE buffer, only the basal membrane sheets remained affixed. For the mCUPs, we employed an adapted method employing a more delicate burst in PBS for 10 min at room temperature (RT) before mounting them using a homemade Mowiol mounting medium.[7]

To identify the cis-Golgi network (GM130), trans-Golgi network (TGN46), and early endosomes (EEA1), we employed immunocytochemistry techniques. Initially, after

cell fixation, permeabilization was achieved by treating the cells with 0.1% Triton X-100 for 20 min. Subsequently, a blocking step was carried out for 1 h using a solution comprising 10% goat serum, 5% nonfat powdered milk, and 0.05% Triton X-100. Following this, the cells were subjected to overnight incubation at 4°C with specific primary antibodies: mouse anti-GM130 (1:1000; BD Transduction Laboratories), rabbit anti-TGN46 2F11 (1:100; BioNova Científica), and mouse anti-EEA1 (1:500; BD Transduction Laboratories) dissolved in 10% goat serum and 0.05% Triton X-100. Subsequent to primary antibody incubation, the cells were treated with either goat anti-rabbit or anti-mouse Cy5-conjugated secondary antibodies for 2 h at RT. Finally, the specimens were mounted using a homemade Mowiol mounting medium for further analysis.

To label the plasma membrane of AC16 cardiomyocytes, a staining of Wheat Germ Agglutinin (WGA) conjugated with Alexa Fluor 555 (Fisher Scientific) was performed. Live cells were incubated on ice for 5 min, followed by three quick washes with cold PBS. Next, cardiomyocytes were stained with a dilution of WGA-Alexa Fluor 555 (1:1500) in DMEM supplemented with 30 mM HEPES for 5 min at 4°C. Cells were washed twice, fixed with paraformaldehyde 4% for 10 min, and mounted as explained before.

4.4 | Immunohistochemistry on human cardiac samples

Auricle specimens from patients were fixed in 4% paraformaldehyde, cryoprotected in 30% sucrose in PBS, embedding in optimal cutting temperature (OCT), and -frozen in liquid nitrogen and stored at −80°C OCT. Samples were sectioned at 5 μm thickness in a cryostat (Leica). The study complies with the Declaration of Helsinki and was approved by the Ethics Committee of the University Hospital Puerta de Hierro–Majadahonda, Madrid, Spain. Written informed consent was obtained from all participants before being included in the study.

The sections were washed with PBS, treated with NH_4Cl 50 mM for 10 min and Zyblack quenching for 5 min (ZytoVision). After permeabilization with 0.2% Triton X-100, samples were blocked with 5% BSA (Bovine Serum Albumin) for 30 min and incubated with rabbit anti-JPH4 (1:100; Alomone) overnight at 4°C. The next day samples were washed with PBS and incubated with a goat anti-rabbit secondary antibody (1:500) conjugated to ALEXA 488 (Invitrogen) for 45 min at RT. For a second immunodetection, the samples were blocked again with 5% BSA and incubated with mouse anti-Kv7.1 (1:400, Neuromab) at 4°C overnight, then washed with PBS and incubated with anti-mouse secondary antibody (1:500) conjugated

to ALEXA 546 (Invitrogen) for 45 min at RT. The nuclei were stained with TO-PRO 3 (1/500; Invitrogen) for 30 min. Finally, the sections were mounted with 50% glycerol in PBS. Negative controls were made without primary antibodies.

Images were collected with a TCS SP5 confocal microscope (Leica) using a 63× HCX PL APO (1.4 numerical aperture) oil-immersion objective. The three channels were sequentially acquired avoiding cross-talk. The following excitation and emission parameters used were (488 nm, 500–540 nm) for the JPH4 signal (546 nm, and 557–572 nm) for Kv7.1 and (633 nm, 645–750 nm) for TO-PRO 3. The gains were adjusted for each channel avoiding saturation in pixel intensity. Z-stacks were obtained from confocal sections at 1 μm intervals. Laser intensity and detector sensitivity settings remained constant for all image acquisitions for experimental replicas. Image processing was performed with the ASF Leica software.

4.5 | Confocal microscopy, Föster resonance energy transfer (FRET), and fluorescence recovery after photobleaching (FRAP)

The examination was conducted using a Leica SP2 laser scanning confocal spectral microscope (Leica Microsystems GmbH) that featured distinct lasers: an argon multiline laser (458, 488, and 514 nm), a diode-pumped solid-state laser (561 nm), and a helium-neon laser (633 nm). Image acquisition for various fluorophores utilized specific laser lines: YFP fluorophore images were captured employing the 514-nm laser, CFP with the 458-nm line, DsRed using the 561-nm line, and Cy5 utilizing the 633-nm line. To accommodate these wavelengths, double dichroic (458/514) and triple dichroic (488/561/633) filters were appropriately employed. Image capture was conducted at a resolution of 1024 × 1024 pixels, employing a 63/1.32 oil immersion objective lens. Scanning incorporated a pinhole aperture set at 1 Airy unit with zoom 4, in adherence to the Nyquist theorem for optimal lateral optical resolution. The scanning process was sequential for observing each fluorescent protein. Post-acquisition, colocalization analysis was performed using Manders′ overlap coefficient (MOC), which is derived from a global analysis of pixel intensity distributions. The coefficient ranges between 0 (indicating no colocalization) to 1 (representing 100% colocalization) for overlapping images. This analysis was facilitated using JACoP (Just Another Colocalization Plugin; https://imagej.nih.gov/ij/plugins/track/jacop.html).

FRET was quantified employing the acceptor photobleaching configuration. The region of interest (ROI)

underwent three scans using the 514-nm line of an argon laser at full 100% power intensity. Both before and after YFP photobleaching, images of CFP and YFP were captured, all sampled at 512×512 pixels with a 12-bit resolution. To compute the FRET efficiency, the formula (FCFPafter–FCFPbefore)/FCFPafter was utilized, where FCFPafter and FCFPbefore represent the fluorescence levels of the cells post- and pre-bleaching, respectively. The loss of fluorescence as a result of the scans was corrected by measuring the CFP intensity in the unbleached cell region. Analysis was performed using ImageJ 1.53 t.

For FRAP experiments, cells were transfected with Kv7.1-CFP alone or with Kv2.1-HA-YFP or JPH4-GFP in Mattek high glass bottom 35 mm dishes (Mattek). Images were acquired 48 h after transfection with an inverted Zeiss LSM880 laser scanning confocal microscope. Briefly, CFP was bleached for 128 ms with a 458 nm line Ar laser at maximum power, and fluorescence was monitored before and after bleaching with a 63/1.4 Plan Apo PH NA Gly immersion objective at zoom 2 acquired every 0.388 s for 1 min and then every 1 s; this method was controlled by Zen Black 2.3 SP1 FP3 software. In pre and post bleaching acquisition, excitation was performed with the 458 nm Ar laser line at 2% and emission was collected from 465 to 515 nm.

4.6 | Superresolution imaging and sample preparation

Animal procedures received approval from both the Ethics Committee of the University of Barcelona and the Animal Ethics Approval Committee of the University of Exeter in compliance with the EEC directive (86/609/EEC). Ventricles from rats were meticulously dissected and promptly frozen in OCT (Tissue-Tek). Cryostat sections measuring 10 µM in thickness were sliced using a Leica CM3050 cryostat and delicately positioned onto pre-cleaned coverslips coated with 0.1% poly-l-lysine (Sigma). Subsequently, these sections underwent blocking using an Image-iT FX signal enhancer (Thermo Fisher Scientific) for 1 h at RT. Primary antibodies targeting Kv7.1 (Santa Cruz Biotechnology) and RyR2 (Thermo Scientific) were applied overnight at 4°C. Following this, the samples were subjected to a 2 h incubation at RT with secondary antibodies conjugated to Alexa Fluor 647 or Alexa Fluor 700 (Thermo Fisher Scientific). Similarly, the preparation of samples for superresolution imaging on autologous systems was performed. HEK 293-transfected cells were prepared 48 h after transfection using the same labeling protocol. The mCUP protocol was carried out in cultured transfected HEK 293 cells residing in 100-mm dishes before labeling. Imaging procedures took place in a switching buffer consisting of 90% glycerol and 100 mM 2-mercaptoethylamine in PBS. To capture dSTORM images, a modified Ti Eclipse inverted fluorescence microscope (Nikon, Japan) was utilized. Subsequent to image acquisition, custom-written PYthon Microscopy Environment software (available at https://bitbucket.org/david_baddeley/python-microscopy) was employed for image processing, event localization, and grayscale rendering. Colocalization analysis was performed as previously described.[31] Briefly, binary masks of positively-labeled regions were calculated by thresholding images of proteins A and B so that the masked area contained 80% of the total labeling intensity. Binary masks were used for analysis as described previously.[31] This analysis generates histograms of the percentage of protein A labeling as a function of the distance to the edge of the nearest region of protein B labeling.

4.7 | Protein extraction, coimmunoprecipitation, biotinylation, lipid raft isolation, and Western blotting

Hearts, freshly obtained from wild-type male Wistar rats, were digested with collagenase and homogenized until cell dissociation. Homogenates were centrifuged for 1 min at $1000 \times g$. Lysis buffer (150 mM NaCl, 50 mM Tris, 1 mM EDTA, 1 mM EGTA, 1 mM $MgCl_2$, and 1% Triton X-100 (pH 7.2)) was added and incubated for 20 min at 4°C until complete disaggregation. Next, samples were centrifuged at $12\,000 \times g$ for 10 min at 4°C. The supernatants were kept as protein extracts and prepared for Western blot analysis.

HEK 293, COS-7, and AC16 cells were washed twice with cold PBS and scraped with 0.5 mL of protein lysis buffer (150 mM NaCl, 50 mM Tris–HCl, 1 mM EDTA, 1% Triton X-100, pH 7.5) supplemented with protease inhibitors (1 µg/mL aprotinin, 2 µM leupeptin, 1 µM pepstatin, 1 mM PMSF). Lysates were homogenized by incubating the samples in an orbital shaker at 4°C for 10 min and further centrifuged at $15\,000 \times g$ for 15 min. Supernatants were collected, and pellets containing cell debris and non-lysed cells were discarded. The protein concentration was analyzed using the Bradford protein assay.

Low-density, Triton-insoluble complexes (lipid rafts) were isolated as previously described.[32] Briefly, after three washes in phosphate-buffered saline (PBS), cells were homogenized in 1 mL of 1% Triton X-100 MBS (150 mM NaCl, 25 mM 2-morpholinoethanesulfonic acid 1-hydrate, pH 6.5), supplemented with 1 mg/mL aprotinin, 1 mg/mL leupeptin, 1 mg/mL pepstatin, and 1 mM phenylmethyl-sulfonyl fluoride to inhibit proteases, and centrifuged at

$3000 \times g$ for 5 min at 4°C. Sucrose in MBS was added to a final concentration of 40%. A 5%–30% linear sucrose gradient was layered on top and further centrifuged (39 000 rpm – 190 000 $\times g$) for 20–22 h at 4°C in a Beckman SW41Ti swinging rotor. Gradient fractions (1 mL) were collected from the top and analyzed by Western blotting.

Coimmunoprecipitation experiments were conducted using transfected HEK 293 cells 48 h post-transfection. The procedure commenced with cell washing, twice with ice-cold PBS, followed by cell lysis in a solution comprising 1% Triton X-100, 10% glycerol, 5 mM HEPES (pH 7.2), and 150 mM NaCl. To isolate total protein samples, this lysate was supplemented with aprotinin (1 μg/mL), leupeptin (1 μg/mL), pepstatin (1 g/mL), and 1 mM phenylmethylsulfonyl fluoride as protease inhibitors. The resulting homogenates underwent centrifugation at 15 000 $\times g$ for 15 min, and the total protein concentration in each supernatant was determined using a Bio-Rad Protein Assay (Bio-Rad). Protein A–Sepharose beads (GE Healthcare) were incubated with an anti-Kv7.1 antibody (Alomone) for 1 h at RT. Once the bead-antibody complexes were established, they were covalently bound using dimethyl pimelimidate (DMP) (Pierce) by incubating with 20 mM DMP for 30 min at RT. Subsequently, the cross-linking reaction was terminated by the addition of 0.2 M glycine (pH 2.5). The cell lysates underwent a pre-clearing step with protein A–Sepharose beads for 1 h at 4°C with gentle mixing. Following this, equal amounts of protein samples (1–2 mg of protein) were subjected to overnight incubation with the bead-antibody complexes at 4°C. After five washes, the proteins bound to the antibody-bead complexes were eluted using 100 μL of 0.2 M glycine (pH 2.5).

Cell surface protein biotinylation was conducted utilizing the Pierce Cell Surface Protein Isolation Kit (Pierce). Initially, cells were subjected to incubation with EZ-Link Sulfo-NHS-SS-Biotin (sulfosuccinimidyl-2-[biotinamido] ethyl-1,3-dithiopropionate) for 30 min. Subsequently, the surplus-free reagent was neutralized following the manufacturer's instructions. The lysates, prepared according to the aforementioned process, underwent overnight incubation at 4°C within NeutrAvidin Agarose columns. Post-incubation, three washes were executed, and the biotinylated surface proteins were eluted using dithiothreitol SDS–polyacrylamide gel electrophoresis (SDS–PAGE) sample buffer.

To prepare for Western blotting, protein samples were readied in 1× Laemmli SDS loading buffer, followed by a 10 min incubation at 65°C. Subsequently, these samples were subjected to resolution through 8 to 10% SDS–PAGE. The separated proteins were then transferred onto Immobilon-P PVDF membranes (Millipore), which were pre-blocked using 5% nonfat powdered milk in PBS containing 0.05% Tween-20 before initiating the immunodetection process. The membranes were immunoblotted with antibodies against Kv7.1 (1:500, Alomone), KCNE1 (1:500, Alomone), Kv2.1, (1:500, Alomone), JPH1 (1:5000, Abcam), GFP (1:500; Roche), β-actin (1:50000, Sigma), Na$^+$/K$^+$ ATPase (Developmental Studies Hybridoma Bank, The University of Iowa), Calnexin (1:500, BD Transduction), Caveolin (1:250, Sigma), Clathrin heavy chain (1:1000, BD Transduction), BIN1 (1:2000, Abcam), SORB2 (1:250, Sigma), HOMER1 (1:500, Sigma), SEPT4 (1:250, Sigma), Sec22b (1:500, Sigma), AMIGO (1:100, NeuroMab), VAP A (1:250, R&D systems), and VAP B (1:1000, R&D systems). After washing, the blots were incubated with horseradish peroxidase (HRP)–conjugated goat anti-rabbit or anti-mouse secondary antibodies (Bio-Rad) and developed using the Immobilon Ultra Plus Western HRP Substrate (Merck Millipore).

4.8 | Transmission electron microscopy

HEK 293 cells underwent transfection with Kv7.1-pCDNA3.1, either with or without Kv2.1-YFP or JPH4-GFP, and were then cultured for 48 h. Following this, fixation was carried out at RT using paraformaldehyde (PFA) and glutaraldehyde. Protein labeling involved the use of polyclonal anti-Kv7.1 (1:500; Alomone) and monoclonal anti-GFP mouse antibodies (1:50; Roche) targeting Kv2.1-YFP and JPH4-GFP, respectively. To tag Kv7.1-pCDNA3.1 and Kv2.1-YFP or JPH4-GFP, goat anti-rabbit and goat anti-mouse secondary antibodies conjugated to 12-nm and 18-nm gold particles were employed. The fixation process comprised a 1 h treatment with 4% PFA and 0.1% glutaraldehyde in 0.1 M PBS, followed by an additional 30 min in 2% PFA. The subsequent steps involved high-pressure freezing cryofixation using liquid N$_2$, cryosubstitution, Lowicryl resin embedding, block polymerization, and ultrathin sectioning at a 60-nm thickness. These procedures were performed in collaboration with the Unitat de Criomicroscòpia Electrònica (CCiT, Universitat de Barcelona). The mounted samples on Formvar-coated grids underwent incubation with 2% uranyl acetate for 15 min and were subsequently immunogold-labeled as previously described. The observations and analysis of the samples were conducted using a Tecnai Spirit 120 kV microscope.

ER-PMjs were first reported in muscle cells.[33] Based on TEM studies, ER-PMjs are characterized as ER regions lying along the PM. In general, the distance between the ER and the PM at ER-PMjs is within 10 to 30 nm. Most times, the ER and the PM align in parallel with a length of about 100–400 nm in many cell types.[34]

4.9 | Proteomic studies

Coimmunoprecipitation experiments were performed with Dynabeads-Protein A® (Life Technologies). Briefly, 2 mg of protein lysate was added to 500 μL of lysis buffer supplemented with protease inhibitors. Samples were incubated for 2 h at RT or overnight at 4°C with Dynabeads® cross-linked to 7.5 mg of anti-GFP antibody (GeneScript). For antibody cross-linking, BS[3] reagent (Thermo Fisher Scientific) was used following the manufacturer's instructions. Immunoprecipitates were washed three times and eluted with the elution buffer provided by the manufacturer. A total of 124 immunoprecipitations were independently performed and stored at −20°C. Elutions were concentrated together by methanol/chloroform precipitation, and the protein pellet was used for HPLC–MS analysis.

The sample was digested with trypsin following standard protocols.[35] Briefly, the sample was reduced with 0.5 mM TCEP (Tris [2-carboxyethyl] phosphine)/50 mM Tris pH 7.4 for 30 min at 37°C and alkylated for 30 min with IAA (iodoacetamide) in the dark. Then, digestion was performed with trypsin (0.1 μg/μL) in 25 mM Tris (pH 7.4), 0.1% SDS at 37°C overnight. The digestion was stopped by adding formic acid. Peptides were extracted with 100% acetonitrile (ACN) and completely evaporated. Samples were reconstituted in 9 μL of 3% ACN and 1% formic acid aqueous solution for MS analysis. Liquid chromatography was performed using a nano-HPLC Eksigent system. HPLC separation was performed with a gradient from 3% to 35% ACN in 0.1% formic acid for 120 min. Peptides were analyzed with a Velos LCQ-Orbitrap mass spectrometer (Thermo Fisher Scientific). Data were processed using Xcalibur 2.1 (Thermo Fisher Scientific) and submitted to SEQUEST software for further analysis with the HUMAN UniProt SwissProt database. These procedures were performed in collaboration with Unitat de Proteòmica (CCiT, Universitat de Barcelona). Cytoscape v3.7.1 software was used. Functional enrichment analysis was performed using Gene Ontology, Reactome Pathways, and KEGG databases.

4.10 | Electrophysiology

For electrophysiology, COS-7 cells were grown in 60-mm culture dishes using Dulbecco's modified Eagle's medium supplemented with 10% (v/v) fetal bovine serum and penicillin/streptomycin (100 U/mL). Transient transfection was performed using Lipofectamine 2000 (Invitrogen) when the cells reached nearly 60% confluence. Cells were transfected with Kv7.1 in pcDNA3.1 (2 μg) together with EBO pcD-Leu-2 (1 μg), Kv2.1 P404 W in pEYFP-C1 (2 μg) or JPH4 in pEYFP-C1 (2 μg).

Currents were recorded employing the perforated (amphotericin B) patch-clamp technique utilizing an Axopatch 200B amplifier (Axon Instruments), following previously established methods.[36] The internal solution contained (in mM) K-aspartate 80, KCl 50, phosphocreatine 3, KH2PO4 10, Mg–adenosine 5′-triphosphate 3, HEPES-K 10, and EGTA 5, adjusted to pH 7.25 with KOH. Amphotericin B (20 mM; Sigma–Aldrich), dissolved in dimethyl sulfoxide, was added to the internal solution to achieve a final concentration of 0.5 mg/mL, as previously reported.[7,37] The composition of the external solution (in mM) comprised NaCl 130, KCl 4, CaCl$_2$ 1.8, MgCl$_2$ 1, HEPES-Na 10, and glucose 10, adjusted to pH 7.40 with NaOH. Junction potentials between the pipette and external solution were about −9 mV. Recorded currents underwent filtering at 1 kHz (using a four-pole Bessel filter) and sampling at 2 kHz. Micropipettes, fabricated from borosilicate glass capillary tubes (Narishige, GD-1), were pulled using a programmable horizontal puller (Sutter Instruments Co.) and then heat-polished with a microforge (Narishige). The micropipette resistance ranged from 2 to 4 MΩ. Data acquisition and analysis were performed using pClamp version 11 software (Axon Instruments). Recordings were conducted at room temperature (21–23°C) with a stimulation frequency of 0.03 Hz. Data analysis, including least squares fitting, and presentation were performed using Microcal Origin 2022 (Microcal Software) and Clampfit 11 programs.

CONFLICT OF INTEREST STATEMENT

The authors declare no conflict of interest.

DATA AVAILABILITY STATEMENT

The data that support the findings of this study are available from the corresponding author upon reasonable request.

ORCID

María Navarro-Pérez https://orcid.org/0000-0001-8106-9787
Angela de Benito-Bueno https://orcid.org/0000-0002-2499-3145
Paula G. Socuéllamos https://orcid.org/0000-0001-7097-1708
Carmen Valenzuela https://orcid.org/0000-0003-3929-1960
Christian Soeller https://orcid.org/0000-0002-9302-2203
Antonio Felipe https://orcid.org/0000-0002-7294-6431

REFERENCES

1. Barhanin J, Lesage F, Guillemare E, Fink M, Lazdunski M, Romey G. K(V)LQT1 and lsK (minK) proteins associate to form the I(Ks) cardiac potassium current. *Nature*. 1996;384(6604):78-80.
2. Sanguinetti MC, Curran ME, Zou A, et al. Coassembly of K(V) LQT1 and minK (IsK) proteins to form cardiac I(Ks) potassium channel. *Nature*. 1996;384(6604):80-83.
3. Etheridge SP, Asaki SY, Niu MC. A personalized approach to long QT syndrome. *Curr Opin Cardiol*. 2019;34(1):46-56.
4. Murray CI, Westhoff M, Eldstrom J, Thompson E, Emes R, Fedida D. Unnatural amino acid photo-crosslinking of the IKs channel complex demonstrates a KCNE1:KCNQ1 stoichiometry of up to 4:4. *Elife*. 2016;5:e11815.
5. Nakajo K, Ulbrich MH, Kubo Y, Isacoff EY. Stoichiometry of the KCNQ1 – KCNE1 ion channel complex. *Proc Natl Acad Sci USA*. 2010;107(44):18862-18867.
6. Plant LD, Xiong D, Dai H, Goldstein SA. Individual IKs channels at the surface of mammalian cells contain two KCNE1 accessory subunits. *Proc Natl Acad Sci USA*. 2014;111(14):E1438-E1446.
7. Oliveras A, Serrano-Novillo C, Moreno C, et al. The unconventional biogenesis of Kv7.1-KCNE1 complexes. *Sci Adv*. 2020;6(14):eaay4472.
8. Wilson ZT, Jiang M, Geng J, et al. Delayed KCNQ1/KCNE1 assembly on the cell surface helps I(Ks) fulfil its function as a repolarization reserve in the heart. *J Physiol*. 2021;599(13):3337-3361.
9. Jiang M, Xu X, Wang Y, et al. Dynamic partnership between KCNQ1 and KCNE1 and influence on cardiac IKs current amplitude by KCNE2. *J Biol Chem*. 2009;284(24):16452-16462.
10. Poulsen AN, Klaerke DA. The KCNE1 beta-subunit exerts a transient effect on the KCNQ1 K+ channel. *Biochem Biophys Res Commun*. 2007;363(1):133-139.
11. Dixon RE, Trimmer JS. Endoplasmic reticulum-plasma membrane junctions as sites of depolarization-induced Ca(2+) signaling in excitable cells. *Annu Rev Physiol*. 2023;85:217-243.
12. Wu DM, Jiang M, Zhang M, Liu XS, Korolkova YV, Tseng GN. KCNE2 is colocalized with KCNQ1 and KCNE1 in cardiac myocytes and may function as a negative modulator of I(Ks) current amplitude in the heart. *Heart Rhythm*. 2006;3(12):1469-1480.
13. Rasmussen HB, Moller M, Knaus HG, Jensen BS, Olesen SP, Jorgensen NK. Subcellular localization of the delayed rectifier K(+) channels KCNQ1 and ERG1 in the rat heart. *Am J Physiol Heart Circ Physiol*. 2004;286(4):H1300-H1309.
14. Jiang M, Zhang M, Howren M, et al. JPH-2 interacts with Cai-handling proteins and ion channels in dyads: contribution to premature ventricular contraction-induced cardiomyopathy. *Heart Rhythm*. 2016;13(3):743-752.
15. Johnson B, Leek AN, Sole L, Maverick EE, Levine TP, Tamkun MM. Kv2 potassium channels form endoplasmic reticulum/plasma membrane junctions via interaction with VAPA and VAPB. *Proc Natl Acad Sci U S A*. 2018;115(31):E7331-E7340.
16. Cohen HA, Zomot E, Nataniel T, Militsin R, Palty R. The SOAR of STIM1 interacts with plasma membrane lipids to form ER-PM contact sites. *Cell Rep*. 2023;42(3):112238.
17. Baraniak JH Jr, Zhou Y, Nwokonko RM, Gill DL. The intricate coupling between STIM proteins and Orai channels. *Curr Opin Physio*. 2020;17:106-114.
18. Maguy A, Hebert TE, Nattel S. Involvement of lipid rafts and caveolae in cardiac ion channel function. *Cardiovasc Res*. 2006;69(4):798-807.
19. Johnson B, Leek AN, Tamkun MM. Kv2 channels create endoplasmic reticulum / plasma membrane junctions: a brief history of Kv2 channel subcellular localization. *Channels (Austin)*. 2019;13(1):88-101.
20. Lee HC, Wang JM, Swartz KJ. Interaction between extracellular Hanatoxin and the resting conformation of the voltage-sensor paddle in Kv channels. *Neuron*. 2003;40(3):527-536.
21. Madhusudana SN, Sundaramoorthy S, Ullas PT. Utility of human embryonic kidney cell line HEK-293 for rapid isolation of fixed and street rabies viruses: comparison with neuro-2a and BHK-21 cell lines. *Int J Infect Dis*. 2010;14(12):e1067-e1071.
22. Perni S, Lavorato M, Beam KG. De novo reconstitution reveals the proteins required for skeletal muscle voltage-induced Ca(2+) release. *Proc Natl Acad Sci USA*. 2017;114(52):13822-13827.
23. Tamkun MM, O'Connell KM, Rolig AS. A cytoskeletal-based perimeter fence selectively corrals a sub-population of cell surface Kv2.1 channels. *J Cell Sci*. 2007;120(Pt 14):2413-2423.
24. Woo JS, Srikanth S, Nishi M, Ping P, Takeshima H, Gwack Y. Junctophilin-4, a component of the endoplasmic reticulum-plasma membrane junctions, regulates Ca2+ dynamics in T cells. *Proc Natl Acad Sci USA*. 2016;113(10):2762-2767.
25. Suda N, Franzius D, Fleig A, et al. Ca2+−induced Ca2+ release in Chinese hamster ovary (CHO) cells co-expressing dihydropyridine and ryanodine receptors. *J Gen Physiol*. 1997;109(5):619-631.
26. Boncompagni S, Thomas M, Lopez JR, et al. Triadin/Junctin double null mouse reveals a differential role for Triadin and Junctin in anchoring CASQ to the jSR and regulating Ca(2+) homeostasis. *PLoS One*. 2012;7(7):e39962.

27. Kang F, Zhou M, Huang X, et al. E-syt1 re-arranges STIM1 clusters to stabilize ring-shaped ER-PM contact sites and accelerate Ca(2+) store replenishment. *Sci Rep*. 2019;9(1):3975.

28. Ahmad M, Narayanasamy S, Ong HL, Ambudkar I. STIM proteins and regulation of SOCE in ER-PM junctions. *Biomol Ther*. 2022;12(8):1152.

29. Ogen-Shtern N, Chang C, Saad H, et al. COP I and II dependent trafficking controls ER-associated degradation in mammalian cells. *iScience*. 2023;26(3):106232.

30. Pani B, Ong HL, Liu X, Rauser K, Ambudkar IS, Singh BB. Lipid rafts determine clustering of STIM1 in endoplasmic reticulum-plasma membrane junctions and regulation of store-operated Ca2+ entry (SOCE). *J Biol Chem*. 2008;283(25):17333-17340.

31. Hou Y, Jayasinghe I, Crossman DJ, Baddeley D, Soeller C. Nanoscale analysis of ryanodine receptor clusters in dyadic couplings of rat cardiac myocytes. *J Mol Cell Cardiol*. 2015;80:45-55.

32. Perez-Verdaguer M, Capera J, Martinez-Marmol R, et al. Caveolin interaction governs Kv1.3 lipid raft targeting. *Sci Rep*. 2016;6:22453.

33. Moore DH, Ruska H. Electron microscope study of mammalian cardiac muscle cells. *J Biophys Biochem Cytol*. 1957;3(2):261-268.

34. Chang CL, Chen YJ, Liou J. ER-plasma membrane junctions: why and how do we study them? *Biochim Biophys Acta, Mol Cell Res*. 2017;1864(9):1494-1506.

35. Shevchenko A, Tomas H, Havlis J, Olsen JV, Mann M. In-gel digestion for mass spectrometric characterization of proteins and proteomes. *Nat Protoc*. 2006;1(6):2856-2860.

36. Moreno C, de la Cruz A, Oliveras A, et al. Marine n-3 PUFAs modulate IKs gating, channel expression, and location in membrane microdomains. *Cardiovasc Res*. 2015;105(2):223-232.

37. Moreno C, Oliveras A, de la Cruz A, et al. A new KCNQ1 mutation at the S5 segment that impairs its association with KCNE1 is responsible for short QT syndrome. *Cardiovasc Res*. 2015;107(4):613-623.

SUPPORTING INFORMATION

Additional supporting information can be found online in the Supporting Information section at the end of this article.

How to cite this article: Serrano-Novillo C, Estadella I, Navarro-Pérez M, et al. Routing of Kv7.1 to endoplasmic reticulum plasma membrane junctions. *Acta Physiol*. 2024;00:e14106. doi:10.1111/apha.14106